
# A PHOTOMECHANICAL INVESTIGATION OF THE ALGOL SOLID PROPELLANT ROCKET MOTOR NOZZLE

## FINAL REPORT

Herbert Becker
Harold Hamilton

Document No. ARA-F-274-8
May 1965

Prepared for

Contract No. NAS1-3975
National Aeronautics and Space Administration
Langley Research Center
Langley Station
Hampton, Virginia 23365

ALLIED RESEARCH ASSOCIATES, INC.
VIRGINIA ROAD • CONCORD, MASSACHUSETTS

TABLE OF CONTENTS


| | Page |
|---|---|
| LIST OF FIGURES | iv |
| SYMBOLS | vi |
| SUMMARY | vii |
| I. GENERAL INTRODUCTION | 1 |
| A. Purpose of Project | 1 |
| B. Broad Outline of Project | 1 |
| C. Photomechanical Analysis | 2 |
| 1. Principles | |
| 2. Use of Technique | |
| II. THEORETICAL ANALYSIS | 4 |
| A. Section Properties | 4 |
| 1. Introduction | |
| 2. Bending | |
| 3. Radial | |
| 4. Comparisons | |
| B. ARA Nozzle Analysis | 6 |
| 1. Pressure Load | |
| 2. Thermal Load | |
| C. AGC Nozzle Analysis | 7 |
| 1. Summary | |
| 2. Comparison with ARA Theory | |
| III. EXPERIMENTAL INVESTIGATION OF TWO-DIMENSIONAL MODELS | 9 |
| A. Material Properties | 9 |
| 1. Epoxy | |
| 2. Magnesium and Aluminum | |
| B. Preliminary Models | 9 |
| 1. Epoxy | |
| 2. Epoxy and Magnesium | |
| 3. Epoxy and Aluminum | |
| 4. Stress Concentration Models | |
| C. Two-Dimensional Models | 10 |
| 1. Bending Tests | |
| 2. Thermal Gradient Tests | |
| 3. Local Pressure Tests | |
| 4. Artificial Stress Concentration Tests | |
| D. Comparison of Theory with Experiment | 13 |
| 1. Bending | |
| 2. Temperature | |

| | Page |
|---|---|
| IV. EXPERIMENTAL INVESTIGATION OF THREE-DIMENSIONAL MODEL | 15 |
| A. Introduction | 15 |
| B. Bonded Polariscopes | 15 |
| 1. Design<br>2. Location<br>3. Construction | |
| C. Fabrication Technique | 16 |
| D. Pressure Testing | 17 |
| 1. Loading Techniques<br>2. Data | |
| E. Exploratory Thermal Loading | 18 |
| F. Correlation of Theory with Experiment | 18 |
| V. CONCLUSIONS | 19 |
| VI. RECOMMENDATIONS | 20 |
| VII. REFERENCES | 21 |

## LIST OF FIGURES


| Figure No. | Title | Page |
|---|---|---|
| 1 | Influence of Modulus Ratio (m) and Percent Reinforcement (g) on stress | 22 |
| 2 | Data for Analysis of Entrance Cone | 23 |
| 3 | Young's Modulus Measuring Apparatus | 24 |
| 4 | Uniform Bending Moment Test | 25 |
| 5 | Uniform Bending Moment Tests (Preliminary Models) | 26 |
| 6 | Stress Concentration Models | 27 |
| 7 | Stress Concentrations Due to Slits | 28 |
| 8 | Two-Dimensional Model Bending Test | 29 |
| 9 | Algol IIA - 55" # Load | 30 |
| 10 | Algol IIB - 55" # Load | 31 |
| 11 | Algol IIA Surface Stresses at Throat Section | 32 |
| 12 | Algol IIB Surface Stresses at Throat Section | 33 |
| 13 | Apparatus for Loading Throat Section | 34 |
| 14 | Algol IIA - 140" # Load | 35 |
| 15 | Algol IIB - 140" # Load | 36 |
| 16 | Algol IIA Locations of Thermal Stress Test Areas and Thermocouple Locations | 37 |
| 17 | Algol IIB Locations of Thermal Stress Test Areas and Thermocouple Locations | 38 |
| 18 | Algol IIA Nozzle Thermal Induced Stress - Area #1 | 39 |
| 19 | Algol IIA Nozzle Thermal Induced Stress - Area #2 | 40 |
| 20 | Algol IIA Nozzle Thermal Induced Stress - Area #3 | 41 |
| 21 | Algol IIA Nozzle Thermal Induced Stress - Area #4 | 42 |
| 22 | Algol IIB Nozzle Thermal Induced Stress - Area #1 | 43 |
| 23 | Algol IIB Nozzle Thermal Induced Stress - Area #2 | 44 |
| 24 | Algol IIB Nozzle Thermal Induced Stress - Area #3 | 45 |
| 25 | Algol IIB Nozzle Thermal Induced Stress - Area #4 | 46 |
| 26 | Block Diagram of Thermocouple Measurement Setup on Thermal Stress Tests | 47 |
| 27 | Temperature Profiles From Thermal Gradient Tests | 48 |
| 28 | Pressure Loading Throat Section | 49 |
| 29 | Pressure Loading Entrance Section | 50 |
| 30 | Location of Stress Concentration Holes | 51 |

| Figure No. | Title | Page |
|---|---|---|
| 31 | Algol IIA Stress Concentrations | 52 |
| 32 | Algol IIB Stress Concentrations | 53 |
| 33 | Comparison of Experimental and Analytical Data for Bending Tests | 54 |
| 34 | Thermal Tests - Comparison of Analytical and Experimental Data | 55 |
| 35 | Three-Dimensional Model with Pressure Closure in Throat | 56 |
| 36 | Algol IIB Nozzle Location of Bonded Polariscopes | 57 |
| 37 | Bonded Polariscope Sub-Assemblies | 58 |
| 38 | Blank for Throat Section | 59 |
| 39 | Blank with Polariscopes Bonded in Place | 60 |
| 40 | Finished Throat Section | 61 |
| 41 | Finished Throat Section | 62 |
| 42 | Magnesium Reinforcement Blank | 63 |
| 43 | Finished Magnesium Reinforcement | 64 |
| 44 | Blank for Expansion Section of Nozzle | 65 |
| 45 | Finished Expansion Section with Longitudinal Polariscope | 66 |
| 46 | Algol IIB Nozzle Components | 67 |
| 47 | Completed Algol IIB Nozzle | 68 |
| 48 | Pressure Closure in Throat | 69 |
| 49 | Test Arrangement for Viewing Circumferential and Throat Area Polariscopes | 70 |
| 50 | Test Arrangement for Viewing Longitudinal Polariscope in Expansion Section | 71 |
| 51 | Stresses in Entrance Section | 72 |
| 52 | Stresses at Circumferential Polariscopes | 73 |
| 53 | Stress at Throat Section | 74 |
| 54 | Stresses at Expansion Section | 75 |
| 55 | Possible Nozzle Redesign Concept | 76 |

## SYMBOLS

| | |
|---|---|
| $\overline{C}$ | constant - function of temperature profile |
| E | Young's modulus (psi) |
| f | material fringe value (psi-in/fringe) |
| g | percent reinforcement (See Fig. 1) |
| h | depth of section (in) |
| K | factor relating stress to pressure loading |
| M | moment (in-lb) |
| m | $E_2/E_1$ |
| n | number of fringes |
| p | pressure (psi) |
| R | mean radius (in) |
| T | temperature differential $^\circ$ F |
| t | thickness of material (in) |
| Z | section modulus per circumferential inch ($in^2$) |
| $Z_o$ | reference section modulus per circumferential inch, $h^2/6$ ($in^2$) |
| $\alpha$ | coefficient of thermal expansion in-$^\circ$ F/in |
| $\beta$ | ratio $\sigma_1/\sigma_o$ |
| $\theta$ | rotation (radians) (Fig. 2b) |
| $\nu$ | Poisson's ratio |
| $\sigma$ | stress (psi) |
| $\sigma_o$ | reference stress (psi) |

Subscripts

| | |
|---|---|
| e, b | effective for bending |
| e, r | effective for radial loading |
| m | model |
| p | prototype |
| 1 | extreme fiber of region 1 of composite model |
| 2 | extreme fiber of region 2 of composite model |

## SUMMARY

A photoelastic investigation was conducted on scaled models of the Algol IIA and IIB rocket engine nozzles to determine pressure and temperature stresses, to compare theory with experiment, and to obtain a physical understanding of the structural behavior of the nozzle. Both two and three-dimensional models were employed in which the Young's modulus ratio of the prototype liner/reinforcement combination was retained.

The major results were the low stresses observed in the three-dimensional nozzle model under internal pressure applied to the entrance cone and extending downstream as far as the throat. The largest ratio of $\sigma/p$ (induced stress/applied pressure) was not observed to exceed 3, whereas the AGC theoretical analysis showed values as large as 70. An explanation of this discrepancy was sought, part of which may be traceable to the section properties of the nozzle assumed by AGC. The current investigation indicated a significant departure from the AGC values. In fact, the data clearly indicated that the nozzle exhibits orthotropic behavior in the sense that the radial and longitudinal stiffnesses differ widely. Also, qualitative data indicate the possibility that bond cementing problems could be an important factor in prototype design.

Two-dimensional models were employed to determine the relation between bending moment and stress throughout a longitudinal section of the nozzle. The experimental data agreed well with the predictions of elementary composite beam theory generated for this purpose. Photothermoelastic investigations (2D) demonstrated that the maximum thermal stresses in the nozzle would be expected at the early stages of firing (within 10 seconds after ignition, according to the temperature data provided by Aerojet-General). These would be more than double the stresses reported by AGC at 45 seconds.

After discussing those results in detail, the report concludes with a recommendation for a new design concept which could lead to a significant improvement in the structural efficiency of the nozzle.

# A PHOTOMECHANICAL INVESTIGATION OF THE ALGOL SOLID PROPELLANT ROCKET MOTOR NOZZLE

## I. General Introduction

### A. Purpose of Project

The Algol IIA engine nozzle was fabricated by the Aerojet-General Corporation (AGC) for the Scout rocket. Because of problems which arose in the performance of that engine nozzle a redesign version, the Algol IIB, has supplanted the IIA. In order to assess the role of structural behavior as a possible contributor to the problems in the IIA (which may have been related to bonding difficulties at the joints of the non-metallic components), and to determine the structural soundness of the IIB, a project consisting of two and three-dimensional photomechanical model investigations and theoretical comparisons was initiated at ARA with the purpose of evaluating pressure and temperature stresses in the prototype nozzle. This is the final report on that project, the progress of which was depicted in monthly status reports.

### B. Broad Outline of Project

Through discussions with NASA the scope of the program was crystallized at ARA. The major goal was acquisition of data pertinent to the prototype IIB engine nozzle. In order to assure relevance of the model data to the prototype structural performance it was necessary to retain the Young's modulus ratio of the non-metallic nozzle/steel reinforcement combination. This was accomplished through use of an epoxy shell/magnesium reinforcement system. In order to extract the pertinent stress information from the magnesium reinforced region of the three-dimensional model of the IIB, it was necessary to develop intricate forms of the relatively new bonded polariscope technique. For establishement of basic data on the structural character of both the IIA and IIB nozzles, supplementary studies were conducted on two-dimensional models of the longitudinal cross sections of the nozzles to evaluate the relation between internal moment and local stress, to determine the character of thermal stress fields induced by a temperature transient applied to the throat, and to ascertain the nature of the stresses induced by local pressure loads. In addition to providing specific data on the nozzle responses, these studies were directed at assisting the evaluation of stress analysis techniques.

## C. Photomechanical Analysis

### 1. Principles

The major effort of this project was on photomechanical model analysis. Photomechanics is the interaction of light with mechanical behavior. The specific field of investigation of force induced static elastic stresses employing polarized light has long been known as photoelasticity. The more general terms of photomechanics includes dynamic studies (strobelasticity), thermal stress analysis (photothermoelasticity), and investigation of the mechanical behavior of viscoelastic structures (photoviscoelasticity), to name a few.

The current project involves both conventional photoelasticity (PE) and the recently developed field of photothermoelasticity (PTE). In these cases stress and fringe order are linearly related through the well-known stress optic law

$$n = (\sigma_1 - \sigma_2)\, t/f \tag{1}$$

in which the material fringe value, f, is determined by mechanical calibration of the model material. For high precision PTE analysis, this coefficient must be determined as a function of temperature. On a boundary, one of the principal stresses could be the pressure which might be applied to load the model, in which case

$$n = (\sigma_1 - p)\, t/f \tag{2}$$

Naturally, on a free boundary, $p = 0$ and

$$n = \sigma_1 t/f \tag{3}$$

### 2. Use of Technique

When a model is geometrically scaled from the prototype, and the mechanical properties (specifically E) are in the same proportion as in the prototype, then the ratio of stress to loading is the same in both model and prototype. For pressure loading, for example

$$(\sigma/p)_m = (\sigma/p)_p = K \tag{4}$$

Since $\sigma_a - \sigma_b = nf/t$, and it is possible to write $\sigma_a = K_a p$, $\sigma_b = K_b p$, $\sigma_a - \sigma_b = (K_a - K_b)p = K_c p$, then

$$K_c = nf/pt \tag{5}$$

for model studies. Therefore, in addition to information on actual stress due to loading (pressure, moment, temperature), pertinent data also appear in this report in terms of the factor K so that prototype behavior may be deduced directly from the model studies. This is particularly convenient since scale factors are not involved.

## II. Theoretical Analysis

### A. Section Properties

#### 1. Introduction

Bending and radial section properties were determined theoretically for comparison with experimental measurements and with the AGC theory. Basic to these determinations is the hypothesis that the nozzle behaves essentially as a series of parallel rings with essentially no axial diffusion of stresses which would tend to warp initially plane sections. Examination of the validity of that hypothesis is implicit in the goals of this project.

#### 2. Bending

The bending section modulus was determined from the geometry shown in Figure 1 utilizing the assumption that plane cross sections remain plane. The consequent linear strain variation and stress distributions are displayed on the figure. For purposes of analysis a reference stress, $\sigma_o$, was selected on the basis of a homogeneous cross section

$$\sigma_o = 6M/h^2 \tag{6}$$

The stress in the composite was then computed for both extreme fibers in terms of $\sigma_o$ using the following relations

$$\sigma_1/\sigma_o = \alpha = \frac{(1-g)^2 + mg(2-g)}{(1-g)^4 + 2mg(1-g)(2-g+g2) + m^2g^4} = \frac{Z_o}{Z_1} \tag{7}$$

$$\sigma_2/\sigma_o = -m\alpha \frac{1 + (m-1)g^2}{1 + (m-1)g(2-g)} = \frac{Z_o}{Z_2} \tag{8}$$

Equations 7 and 8 are plotted in Figure 1 as a function of percentage reinforcement, g, and modulus ratio, m.

One of the more significant results is the indication of the relative insensitivity of bending stresses to the Young's modulus ratio. As shown in Figure 1, $Z_1/Z_o$ would have an average value of 1.6 in the range of interest so that a representative value for $\sigma_1/\sigma_o$ would be 0.6 over a range of $10 < m < 18$ with less than 10 percent

variation over a wide range of g. A corresponding percentage variation in $\sigma_2/\sigma_o$ may be noted for the same range of m. A representative value for $Z_2/Z_o$ would be 0.4.

### 3. Radial

Through straightforward application of Lame' theory for a composite narrow ring (R >>t) the outside fiber circumferential stress due to pressure may be written

$$\sigma = (pR/t)(1 + E_1t_1/E_2t_2)^{-1} \tag{9}$$

However, when the inner and outer radii differ significantly, Equation 9 must be modified. If the simplified form of Equation 9 is desirable, the radius ratio should be included for reasonable accuracy,

$$\sigma = (pR/t)(1 + R_2^2 E_1t_1/R_1^2 E_2t_2)^{-1} \tag{10}$$

where $R_1$ and $R_2$ are the mean radii of the inner (Region 1) and outer (Region 2) rings, respectively.

The precise form is obviously more complex involving the radii of the inner contour, the interface, and the outer contour of the composite.

### 4. Comparisons

On the basis of the elastic and geometric data for the prototype and for the models of this investigation, a comparison was made of the theoretical $\sigma/\sigma_o$. The range of data reveal the models to represent reasonably well the structural behavior of the prototype.

A comparison of the effective thicknesses for bending and radial behaviors is instructive. If $E_2/E_1$ is chosen as 13 (for the photoelastic model) and a value of 6 is selected for $t_1/t_2$, then the simplified effective reinforcement thickness for the radial behavior would be, from Equation 10,

$$t_{e,r} = t_2 (1 + E_1t_1/E_2t_2) \tag{11}$$

or

$$t_{e,r} = t_2(1 + 6/13) = 1.46t_2 \tag{12}$$

From the standpoint of bending rigidity,

$$E_2 (t_{e,b})^3/12 = E_1 y_1 Z_1 \tag{13}$$

or, after some algebra,

$$t_{e,b} = 4.2 t_2 \tag{14}$$

These two results indicate the large difference between the effective radial and longitudinal thicknesses of the reinforced nozzle. Orthotropic behavior is more to be expected than the simple isotropic behavior assumed by AGC in the analysis of Reference 1.

## B. ARA Nozzle Analysis

### 1. Pressure Load

A highly simplified calculation was made for comparison with the photoelastic observations of pressure induced longitudinal stress in the entrance cone. The loading and geometry are shown in Figure 2. The theoretical value of stress at the location shown in the figure for an assumed pressure of 10 psi was found to be 40 psi ($K = \sigma/p = 4$). Through use of the elastic photomechanical law, $n = \sigma t/f$, the fringe order at that location was calculated to be 0.2 in a bonded polariscope slice 1/4 in. thick.

### 2. Thermal Load

Thermal stresses which were induced in two-dimensional models of the nozzle cross section principally represented thermal shock behavior for the duration of loading. The three-dimensional (or axisymmetric) stress may be found from the relation

$$\sigma = \overline{C} \alpha E T \tag{15}$$

where the value of $\overline{C}$ depends upon the shape of the temperature profile and the geometry of the structure.

A representative value for $\overline{C}$ at an early stage of thermal shock on a 2D model would be 0.8, based on data acquired during numerous PTE investigations. Actually, the value of $\overline{C}$ would change from 1 to 0 during a long transient on the edge of a 2D model and from $(1 - \nu)^{-1}$ to 0 on the surface of a 3D model.

The 10 second temperature field in the prototype involves a temperature in the order of 4000F. Using the appropriate values for $\alpha$, E and $\nu$ for the graphite insert,

$$\sigma = 0.8 \times (2 \times 10^{-6}/F)(2 \times 10^{6}\text{psi})(4000F)/(1 - 0.25)$$

or $$\sigma = 16,000 \text{ psi (compression at the throat)}$$

## C. AGC Nozzle Analysis

### 1. Summary

Pressure stress analysis of the Algol nozzles was performed through use of a ring type computer program on the steel reinforcement with and without modifications to the metal thickness to account for the presence of the refrasial and carbon. Furthermore, the thickness increase which was confined to the inlet cone, was selected equal to

$$\Delta t_2 = (E_1/E_2)t_2 \qquad (16)$$

On this basis, K (computed from the AGC stresses) was found to be 70 for the unthickened reinforcement and 60 for the thickened reinforcement.

Thermal stresses were computed at three transverse sections of the nozzle on the assumption of long cylinder behavior considering interaction between the carbon and metal. Temperatures were calculated using transient axisymmetric heat transfer. Stresses were determined for the temperature distribution at 10 and at 45 seconds after startup, for which times AGC reported peak axial stresses of 8650 psi and 8500 psi, in the carbon.

### 2. Comparison with ARA Theory

The following table summarizes the theoretical ongitudinal nozzle stresses as computed by AGC and by ARA

| | AGC (Ref. 1) | ARA | $\frac{\sigma_{ARA}}{\sigma_{AGC}}$ |
|---|---|---|---|
| Pressure (K) (Entrance cone) | 70 | 4 | 0.06 |
| Temperature* $\sigma$(psi) | 8650 (10 sec. after startup) | 16,000** | 1.9 |

*Throat
**Thermal Shock, Any Location

As may be seen in the last column, the highly simplified ARA analysis predicts pressure stress considerably lower than those predicted by AGC in Reference 1. On the other hand, thermal stresses show the opposite relation. However, these latter values pertain to different times. The AGC stresses are related to a more diffuse (radially) temperature field than those calculated by ARA. In this latter case, the interaction with the reinforcement would be small at such a short time after startup whereas the 45 second temperature field would induce significant stresses in the metal. Consequently, it is not possible to relate metal stresses in the same manner as the throat stresses computed from these analyses.

## III. Experimental Investigation of Two-Dimensional Models

### A. Material Properties

#### 1. Epoxy

The data on model material properties were obtained at the start of the investigation. Young's modulus for the Hysol 4290 plastic used in these experiments was determined from a load-deflection test using a dual objective microscope and a pneumatic universal testing machine both of which were developed by ARA. A photograph of the experimental arrangements for these measurements is presented as Figure 3. Young's modulus for the material used in this program was determined to be 505,000 psi.

The material fringe value at room temperature of the Hysol 4290 plastic was measured by loading a disk in diametral compression and recording the forces required to produce integral fringe orders at the center of the disk. The material fringe value, f = 53.0 psi-in/fringe, was determined from the slope of the line faired through the data.

The Young's modulus and material fringe value variation with temperature were considered using data of accuracy sufficient for this program. These data were obtained on earlier ARA work in photothermoelasticity analysis.

#### 2. Magnesium and Aluminum

During the course of this program, the Young's modulus values used were 10,500,000 psi for aluminum and 6,500,000 psi for magnesium.

### B. Preliminary Models

#### 1. Epoxy

A broad understanding of the stress distribution in a composite structure can be obtained from examination of the simplest structure that can be derived realistically from the actual model. Working from this premise a preliminary two-dimensional model of a longitudinal slice thru the Algol IIB nozzle was fabricated from a sheet of photoelastic plastic. This model was subjected to a uniform moment load using the experimental arrangement of Figure 4. The resulting fringe pattern, as viewed in a dark field polariscope, is shown in Figure 5a. It is typical of beam behavior, even in the neighborhood of the nozzle throat. The shallow entrance cone and rapidly changing wall thickness in the throat region do not appear to have altered significantly the general beam characteristic of the stress distribution.

2. Epoxy and Magnesium

The longitudinal section of the Algol IIB preliminary model was modified to represent the prototype more closely by adding a magnesium insert to simulate the stiffness of the steel housing of the prototype nozzle. The combination of magnesium and plastic resulted in a model with m = 13.

The uniform moment test was performed on this model and produced the stress distribution depicted by the fringe patterns in Figure 5b. Once again, the general bending stress distribution is evident.

3. Epoxy and Aluminum

In order to examine experimentally the dependence of the stress distribution on the modulus ratio of the component materials, the model was modified again by removing the magnesium insert and replacing it with an aluminum insert. This modification changed m from 13 to 20. The fringe pattern for this configuration, shown in Figure 5c, was produced by the same uniform moment load used for the first two models. Hardly any difference from the pattern of Figure 5b may be observed. This result would conform with the prediction of Section IIA.

4. Stress Concentration Models

In this experimental stress analysis on a composite structure with bonded components it was felt to be of design significance to determine whether possible trouble may result from the stress concentrations which would be caused by local failure of the bond between components. This condition was investigated by making saw cuts in the preliminary aluminum/epoxy model as shown in Figure 6. After the first cut, the model was subjected to a moment load, generating the fringe pattern shown in Figure 7a. A second cut was made elongating the slit to one inch, after which the model was retested under the same loading condition yielding the fringe pattern depicted in Figure 7b.

C. Two-Dimensional Models

1. Bending Tests

Based on the confirmation obtained from the preliminary models on the reliability of a composite magnesium/epoxy model, two-dimensional models of a longitudinal section of the Algol IIA and Algol IIB nozzles were made from type AZ31B magnesium and Hysol 4290 epoxy. The models were subjected to a series of precisely controlled moment loads while in a polariscope to provide data for determining

the relation between moment and stress throughout the longitudinal sections, and to permit accurate correlation of theory and experiment.

The models were loaded in the experimental arrangement shown in Figure 8. The supports for the model in this experiment were suspended from pivot points to allow lateral motion as it bent under the application of the moment load, thereby preventing a spurious loading from the model supports. The loading forces were generated by dead weights.

The tests were performed with the model placed in a dark field circular polariscope, illuminated with uniform white light. Fringe pattern photographs were taken through an interference filter which transmits a sharp band at 5461 Å.

The first series of tests provided satisfactory stress information in the entrance and expansion cone regions of the models, but the stresses in the throat area were too low to yield accurate distributions employing the fringe interpolation method. This condition can be seen in the fringe patterns depicted in Figures 9 and 10 which were generated by 55 in-lb moments. Larger moments than this were not applied to the models in this arrangement in order to avoid creep and possible failure at the exit cone location.

Since the stress distribution in the throat area produced low fringe orders, accurate data were obtained at the inner edge of the model with a Babinet compensator which permits fringe order measurement precision well within 1 percent. The edge stress distribution obtained from the Babinet compensator reading is given in Figure 11 for the Algol IIA model and in Figure 12 for the Algol IIB model. In order to obtain a higher level of stress in the throat area without overstressing the thinner areas of the model, the experimental arrangement was changed by adding a fitting to apply the moment load near the throat section as can be seen in Figure 13.

Moment loads up to 140 in-lb were applied with this test arrangement which induced fringe orders high enough to reveal clearly the nature of the stress distributions in the throat area and the inlet area, as can be seen in Figure 14 for the Algol IIA model and in Figure 15 for the Algol IIB model.

### 2. Thermal Gradient Tests

For convenient application of the thermal input to the two-dimensional models of the longitudinal sections of the IIA and IIB, the models were divided into the four regions shown in Figures 16 and 17 for thermal gradient tests. Each area was tested

separately by supporting it uniformly from below and applying a shaped piece of dry ice to the upper surface with a 1/16 in. thick piece of silicone rubber between the ice and the plastic to reduce the thermal shock at the edge of the plastic. If the thermal shock were not diminished in this manner, the fringes generated in the plastic would have been so closely spaced that definition would have been diminished with consequent loss in reliability of the reduced data.

The fringe pattern photographs were taken at 1/2, 1, 2, 4, and 6 minutes after the application of the dry ice. Results for the Algol IIA model are presented as Figures 18 through 21, and for the Algol IIB, in Figures 22 through 25.

Upon completion of the thermal input test series in which photoelastic fringe pattern photographs were taken, the series was rerun to check the temperature distributions, although experience with photothermoelasticity has always revealed excellent correlation of stresses with temperature profile data. Thermocouples were implanted in the models as shown in Figures 16 and 17. A schematic drawing of the apparatus used to measure and record the temperature data is presented in Figure 26. The temperature profiles are shown in Figure 27 for four stations on the IIA and the IIB models.

### 3. Local Pressure Tests

The influence of reinforcing material on the stress distributions in the nonmetallic components of the nozzle was investigated by local pressure experiments which were designed specifically to test the longitudinal "smearing" action of the local stress field by the metallic reinforcement. The model was placed with a section of the outer surface resting on a rigid support and a uniform pressure was applied through a load distributing pad at the corresponding section of the inner surface. Each model was loaded at the entrance section and at the throat section. The fringe patterns resulting from these tests appear in Figure 28 for throat sections and Figure 29 for entrance sections. There is little evidence of smearing or stretching of the fringes in the plastic adjacent to the magnesium reinforcement.

### 4. Artificial Stress Concentration Tests

In order to determine the influence of cement failures in the bonded areas of the inserts of the prototype nozzle, small holes were drilled in the two-dimensional models as shown in Figure 30. It was felt that a hole would provide a more reliable indication of debonding sensitivity than an arbitrary slit of uncertain character.

The models were loaded to 69.6 in-lb in the test apparatus shown in Figure 13. Fringe pattern photographs of the unloaded and loaded model of the Algol IIA are shown in Figure 31 and of the Algol IIB in Figure 32. There is little doubt that weaknesses at the entrance and exit cone cemented joints in the prototype would tend to propagate in these areas adjacent to the carbon insert if high tensile stresses were to occur at those locations.

One of the most interesting results is the observation of local stresses in the plastic at the magnesium insert, visible in Figure 31. These joints were made with epoxy cement, although probably of a composition different from the cement employed on the prototype. The local stresses induced by cementing of epoxy models are a well-known effect in photoelasticity. Even through exercise of extreme care these stresses cannot always be eliminated. There may be significance of this result to the prototype fabrication process.

## D. Comparison of Theory with Experiment

### 1. Bending

The theoretical relation between stress and moment appear in Figure 33 together with the stress distribution obtained from reduction of the fringe pattern data. Considering the rapid changes in section of both the plastic and reinforcement, the shortness of the beams in each section, the more or less arbitrary choice of section orientation, and the abrupt beginning and termination of the reinforcement, reasonable agreement is indicated in the entrance cone and throat regions. Downstream excellent correlation of theory and experiment is evident.

### 2. Temperature

Past experience in photothermoelasticity has shown consistently excellent agreement of experimental data with theoretical stresses based on temperature distributions. Consequently, it was felt necessary only to conduct check temperature measurements and to correlate the data with approximate temperature profiles to establish agreement of stress profiles with temperature fields. The stresses determined photothermoelastically compared favorably with theoretical stresses determined for the thermal shock portion of the temperature cycle where the temperature gradient near the edge usually conforms to an exponential distribution.

$$T = T_o e^{-kx} \qquad (17)$$

Comparisons were made with the experimental data by first converting the photothermoelastically measured stresses into temperatures with the aid of the thermocouple data, as shown in Figure 34. The shape of that temperature distribution was then compared to an exponential decay in the thermal shock region near the chilled edge of the model. Good agreement was obtained, as may be seen in the typical example of Figure 34.

## IV. Experimental Investigation of Three-Dimensional Model

### A. Introduction

Because of the problems of stress freezing a composite epoxy/magnesium model, three-dimensional testing was conducted at room temperature utilizing bonded polariscopes in selected locations to reveal the character of the stress distribution. The three-dimensional photoelastic model was an accurate 1/4 scale reproduction of the prototype Algol IIB using Hysol 4290 epoxy for the refrasil insulator, carbon throat and fiberglas filled epoxy wrap. The steel reinforcement of the prototype was duplicated in Type AZ31B magnesium alloy. A drawing of the photoelastic model is shown in Figure 35.

Fabrication and experimentation on this model consumed the major portion of the investigation. The production of the model required coordination of rough machining, construction and placement of bonded polariscopes, finish machining of the entrance cone and throat region, reinforcement, exit cone, and plexiglas sleeve; cementing of these components; and final finishing of details for test such as attachment of pressure lines. The details are discussed in the following sections.

### B. Bonded Polariscopes

#### 1. Design

Light field circular polariscopes were chosen for mechanical and photoelastic reasons. Mechanically, a light field polariscope can be made from a pair of single sheets of commercially available circularly polarizing plastic. A dark field polariscope would require an extra piece of plastic with two additional bonding surfaces. Photoelastically, a circular polariscope is desirable because is suppresses the isoclinic pattern which is superimposed on the isochromatic pattern in a plane polariscope.

The two general stress fields of most interest in a structure of this type are circumferential stresses (which can be seen in a polariscope embedded in the model on a plane transverse to the central axis of the nozzle) and bending stresses (which are revealed in a polariscope embedded parallel to the central axis). The transverse polariscopes are easiest to embed in the model because a direct line of sight is available through the polariscope for illumination and viewing. On the other hand, the line of sight through the longitudinal polariscope is blocked by the metal housing of the model. This requires inclusion of mirrored surfaces bonded within the model so that, by the use of supplementary external mirrors, the fringe pattern can be observed by looking along the axis of the model.

2. Location

After studying the data obtained in the early stages of the investigation, and following discussions with NASA, it was decided to place circumferential polariscopes at the throat area of the nozzle and at the expansion end of the metal reinforcement. A series of longitudinal polariscopes extended the length of the model from the flange at the inlet section to two inches beyond the end of the metal housing in the expansion portion of the nozzle. The polariscope locations are depicted in Figure 36.

3. Construction

The bonded polariscopes were fabricated as subassemblies employing a plate 1/4 inches thick cut from the same plastic material as the model, and circular polarizer type HNCP-37 cemented to each face of the plastic plate (Figure 37). The longitudinal polariscopes required the addition of another block of plastic cemented to one side with a flash silver reflector at 45°. These subassemblies (Figure 37) were cemented and cured before insertion into the model. The rough machined entrance and exit cones were cut to receive these subassemblies, which were cemented into place before finish machining began.

C. Fabrication Technique

In order to obtain the stress distribution associated with the basic shapes of the prototype nozzle, it was decided to manufacture the nozzle model with a minimum number of bonded joints. To accomplish this objective the inlet and throat area of the nozzle were machined as one piece from a solid block of epoxy.

Figures 38 through 41 show this section of the model in stages of completion. Figure 38 shows the roughed out block of the section. In Figure 39 the section has been cut and the polariscope segments have been bonded in place. Figures 40 and 41 display the entrance cone and throat region with all polariscopes in place and ready to be cemented into the finished assembly.

Figures 42 and 43 depict the blanked and finished magnesium housing element of the nozzle.

The blank from which the expansion cone was fabricated is depicted in Figure 43 and a view of the finished cone, including the downstream portion of the longitudinal polariscope, appears in Figure 45.

A spread out view of the entire nozzle prior to the final bonding operation is shown in Figure 46. Figures 47 and 48 depict the completed nozzle.

## D. Pressure Testing

### 1. Loading Techniques

To simulate the pressure loading applied during hydrostatic test of a prototype nozzle, the plexiglas cylinder was fabricated and installed in the throat section of the model as shown in the drawing of the complete model (Figure 35) and in the end view of the model (Figure 48). Plexiglas end plates were bolted to the magnesium housing to close the inlet end of the nozzle and to simulate the constraint imposed by the end closure of the rocket.

The model was tested with pneumatic pressure as shown in Figures 49 and 50. Figure 49 depicts the arrangement for photographing both circumferential polariscopes, and the longitudinal polariscope up to the throat of the model. In order to photograph the portion of the longitudinal polariscope which extended beyond the metal housing into the expansion section of the nozzle, the model was placed in a Halowax/paraffin fluid filled plexiglas tank. The index of refraction of the fluid was matched to the epoxy. This precaution was necessary to prevent distortion of a fringe pattern due to refraction of light at the surface of the model. The photograph ot the tank assembly appears in Figure 50.

A further precaution was taken to avoid accidental failure of the model at the low strength silver flashed internal mirror surface near the longitudinal bonded polariscope. This was accomplished by limiting the model pressure to 50 psi maximum. Actually, most of the pressure data were recorded at 30 to 40 psi.

### 2. Data

Color photographs were taken of the fringe patterns in the polariscope at zero pressure and at a test pressure of 40 psi. Figure 51 depicts the fringes revealed by the longitudinal polariscope in the entrance section of the nozzle. A low level fringe order is evident in the zero pressure photograph which indicates a residual stress generated by the bonding process. This fringe order increased with the applied pressure and was the highest stressed point found in the model.

Figure 52 shows the circumferential polariscopes loaded and unloaded. There were no discernable fringe patterns generated in the test. Figure 53 depicts the longitudinal polariscopes in the throat area. The photograph taken during the pressure test reveals an increase in fringe order of approximately 0.1 under a pressure rise of 40 psi. The test made to observe the stress in the longitudinal polariscope in the expansion section of the nozzle showed no observable increase in the fringe order as can be seen in Figure 54.

E. Exploratory Thermal Loading

In order to explore the general nature of the three-dimensional thermal stress field. Halowax oil was cooled to 50F and was then poured rapidly into the entrance cone of the model while it was in the upright position shown in Figure 50. The fringe order observed in the model was of the order of 3/4 to 1.

With the model initially at 72F, this provided 22F temperature difference which theoretically would have induced a peak circumferential thermal stress in the epoxy of 275 psi according to Equation 15 using $\overline{C} = 1/2$ as a representative value based on past experience. Since the polariscope thickness was 1/4 in., then the theoretical fringe order would have been 275 x 1/4/55, or 1.25.

A more precise value of $\overline{C}$ would require the addition of thermocouples to the model to obtain accurate temperature profiles as functions of time, followed by accurate thermoelastic analysis.

F. Correlation of Theory with Experiment

The elementary ARA theoretical stress analysis of Section IIB1 agreed in order of magnitude with the experimental observations of the three-dimensional investigation, whereas the AGC theory of Reference 1 over-estimated the stresses by a factor of 18. The implication to be extracted from this result is the large underestimate, by AGC, of the longitudinal bending stiffness of the nonmetallic components of the nozzles. A theoretical comparison of the bending and radial properties was presented in Section IIA4 on the basis of the elementary ARA theory.

In deriving the relation in Section IIB1 for the theoretical stress in the nozzle, it was assumed that the outer periphery (at the attachment to nozzle flange) was clamped. However, an approach to a completely clamped condition is seldom attained at a bolted connection. The relatively good agreement of the experimental result with the elementary theory can only be interpreted as agreement of the observed and theoretical structural behaviors. The fringe orders were too low to permit a more significant interpretation.

## V. Conclusions

1. The results of the two-dimensional investigations indicate that a useful theoretical stress analysis could be made of a metal reinforced nozzle if it were to be considered an orthotropic shell with radial and circumferential section properties determined as shown in Section IIB1 of this report.

2. The low stress ratios which were found experimentally indicate the nozzle may be overdesigned if it were to be considered a homogeneous nonmetallic shell reinforced by a metal sleeve. The effect of cemented connections of components which comprise the actual nozzle, however, may change the useful strength considerably. The cemented connections appear to have been made in regions of maximum tension stress arising from the internal pressure.

3. The AGC theory of Reference 1 appears to be unduly conservative as a means of estimating the nozzle strength as a homogeneous shell. Furthermore, questionable estimations appear to have been made of the proper longitudinal bending cross section properties in developing that theory.

4. The maximum thermal stress in the nozzle, according to the time/temperature data in the AGC theoretical analysis, would have occurred 10 seconds after ignition as a thermal shock. The peak stress at that time would have been expected to be double the value reported theoretically by AGC, which pertained to 45 seconds after ignition.

5. Residual stresses from component bonding may initiate problems in the prototype where less control is possible than in fabrication of the scale models.

## VI. Recommendations

1. Pressure and temperature loadings should be increased to obtain more accurate stress data. For this purpose the plexiglas sleeve should be removed to represent more closely the condition existing in the prototype.

2. Comparison of the experimental data on the actual model, using model material properties, should be made with a more accurate theory. Presumably this is available in the method described by Wilson in Reference 2.

3. A study should be conducted of the possibility of utilizing a modeling procedure which circumvents the laborious and expensive three-dimensional method. One possibility appears to lie in the use of a technique for simulating the elastic foundation approach to the analysis of shell behavior under local bending.

4. Consideration may be given to alternate design concepts. The purpose of such a study would be to evolve construction techniques which could take full advantage of the strength of the nozzle without penalties instituted by weak connections. One such possibility is shown in Figure 55 as a schematic representation. The locations and orientations of the nonmetallic connections are shown in a manner which emphasizes the minimum interference which they could exert upon the basic strength of the nozzle. It is felt that a program of design concept development with such a goal would be a worthwhile extension of the steps taken in this project.

## VII. References


1. Pfluger, W. D., M. L. Hodgens and R. D. Entz, "Final Stress Report on the Algol IIA Nozzle Assembly," Aerojet General Corporation, 13 December 1963.

2. Wilson, E. L., "Structural Analysis of Axisymmetric Solids," Paper 65-143, presented at the AIAA Second Aerospace Sciences Meeting, New York, N. Y., January 25-27, 1965.

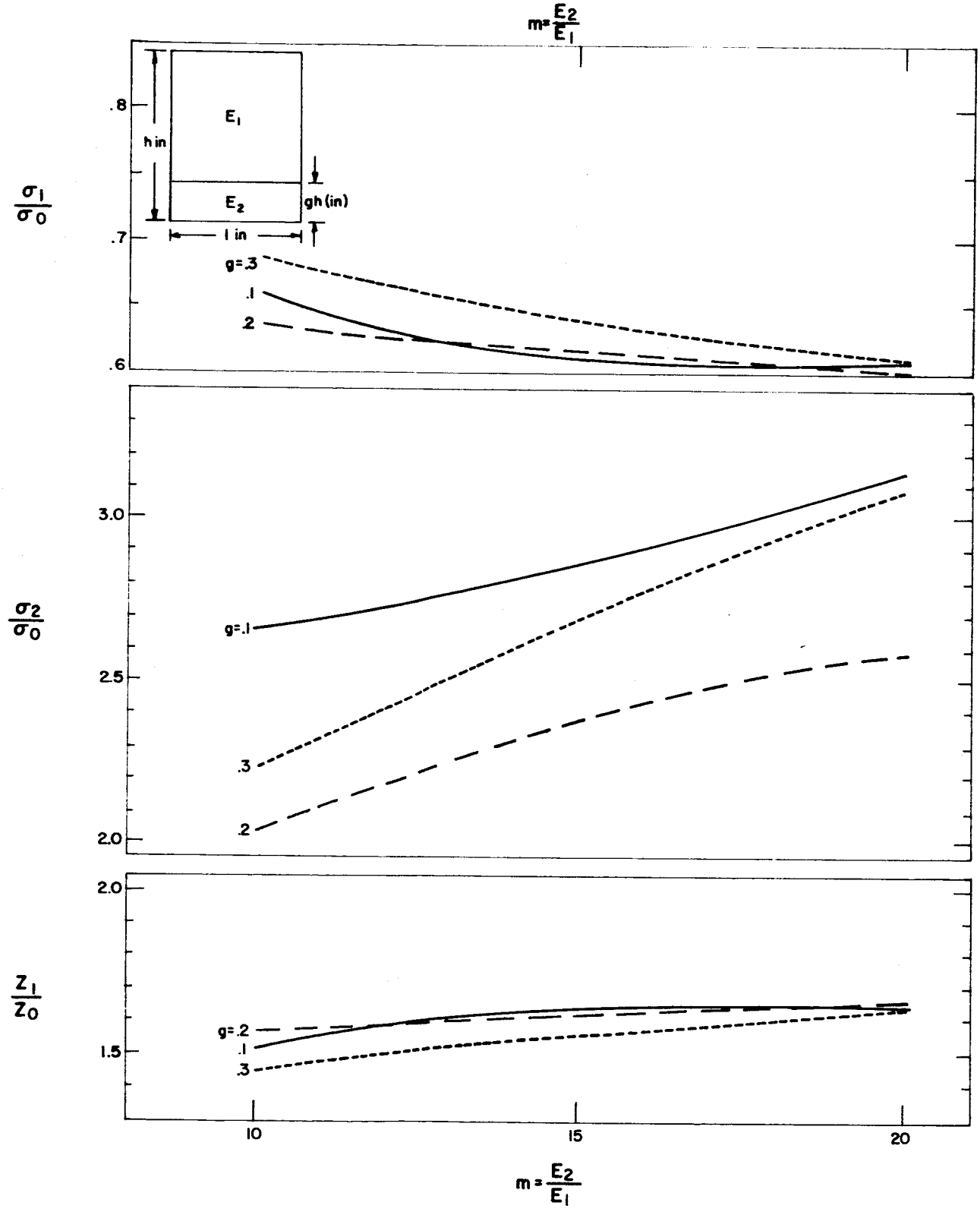


FIG. 1

# INFLUENCE OF MODULUS RATIO (m) AND PERCENT REINFORCEMENT (g) ON STRESS

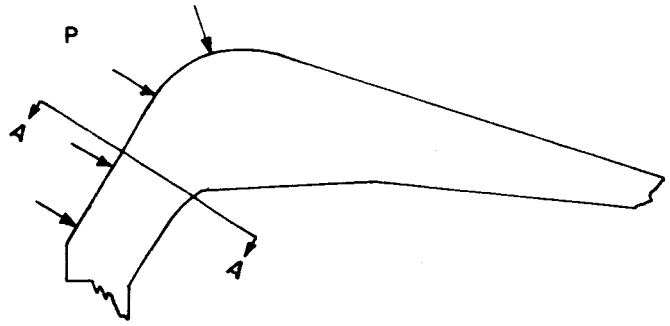


a. THREE-DIMENSIONAL MODEL AT ENTRANCE CONE

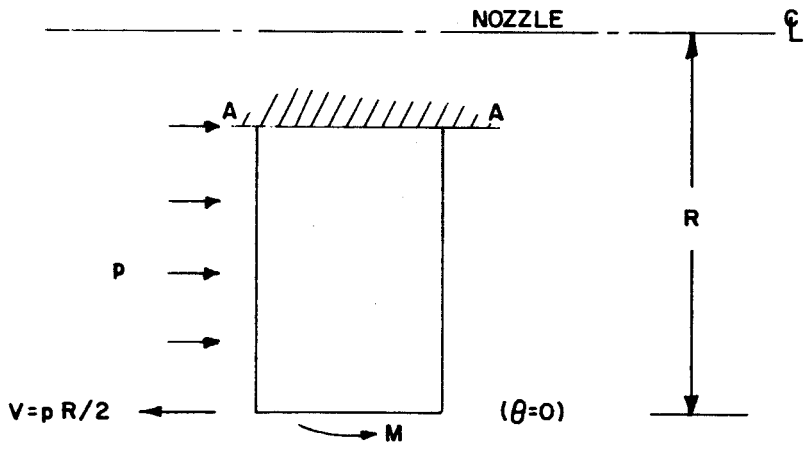


b. SIMPLIFIED TWO-DIMENSIONAL STRUCTURE USED IN ARA ANALYSIS (ASSUMED THICKNESS = 1 in.)

FIG. 2

# DATA FOR ANALYSIS OF ENTRANCE CONE

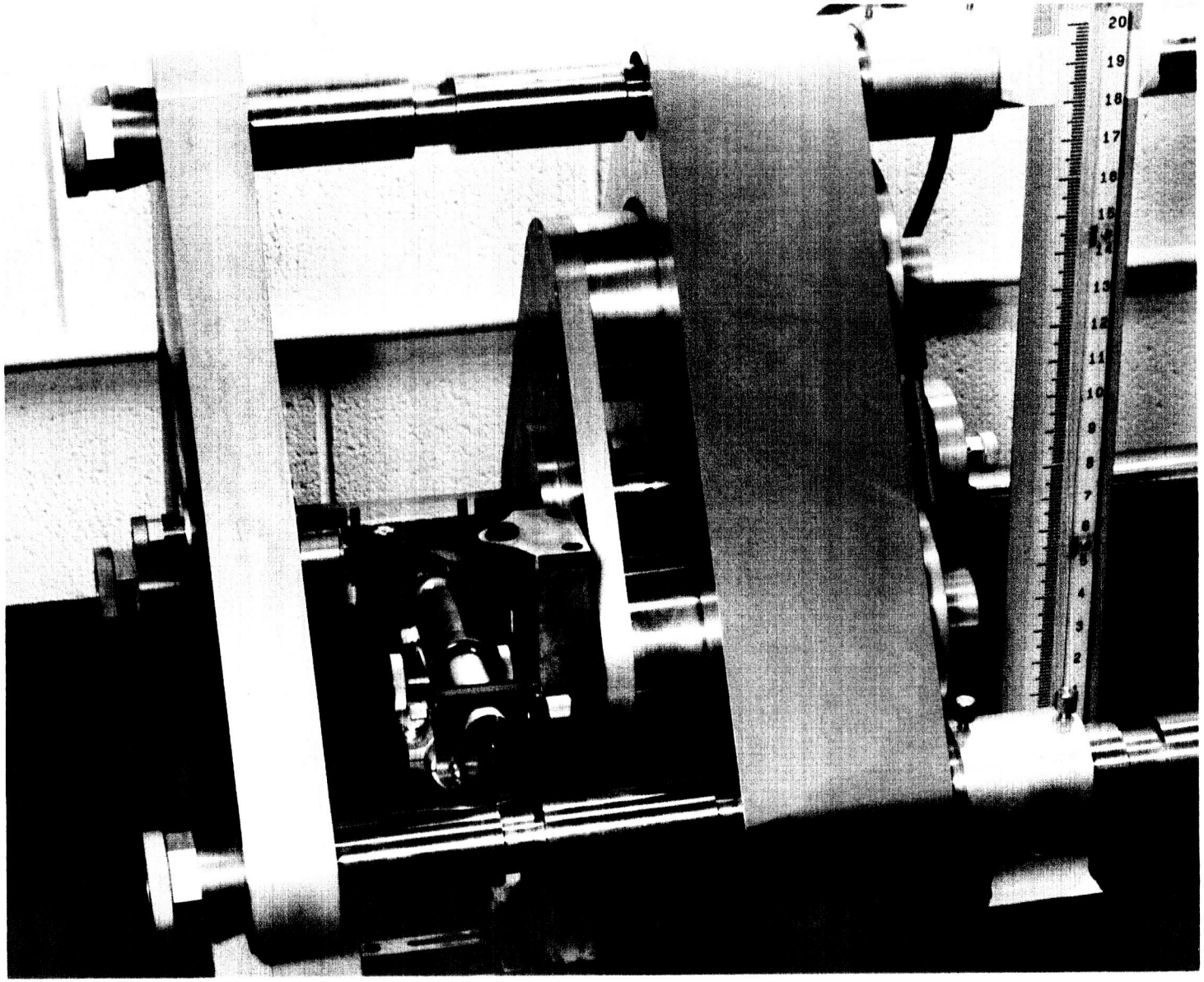


FIG. 3

YOUNG'S MODULUS MEASURING APPARATUS

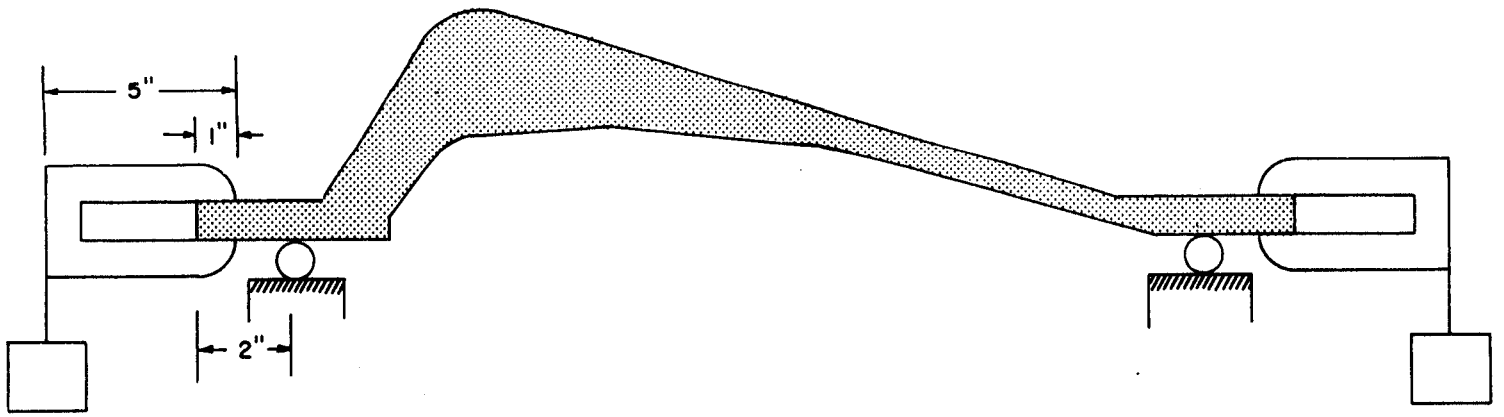


FIG. 4

UNIFORM BENDING MOMENT TEST

FIG. 5

# UNIFORM BENDING MOMENT TESTS

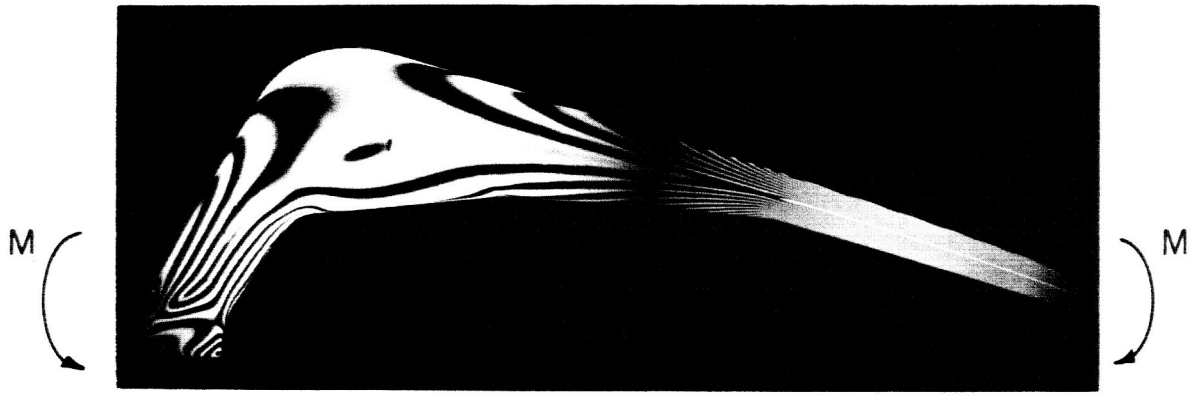


a. SOLID EPOXY MODEL


b. MAGNESIUM INSERT

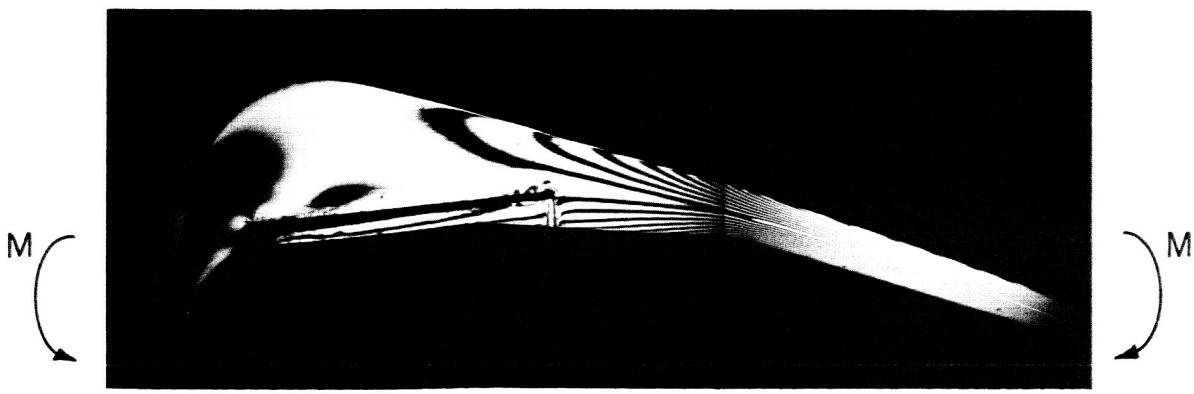


c. ALUMINUM INSERT

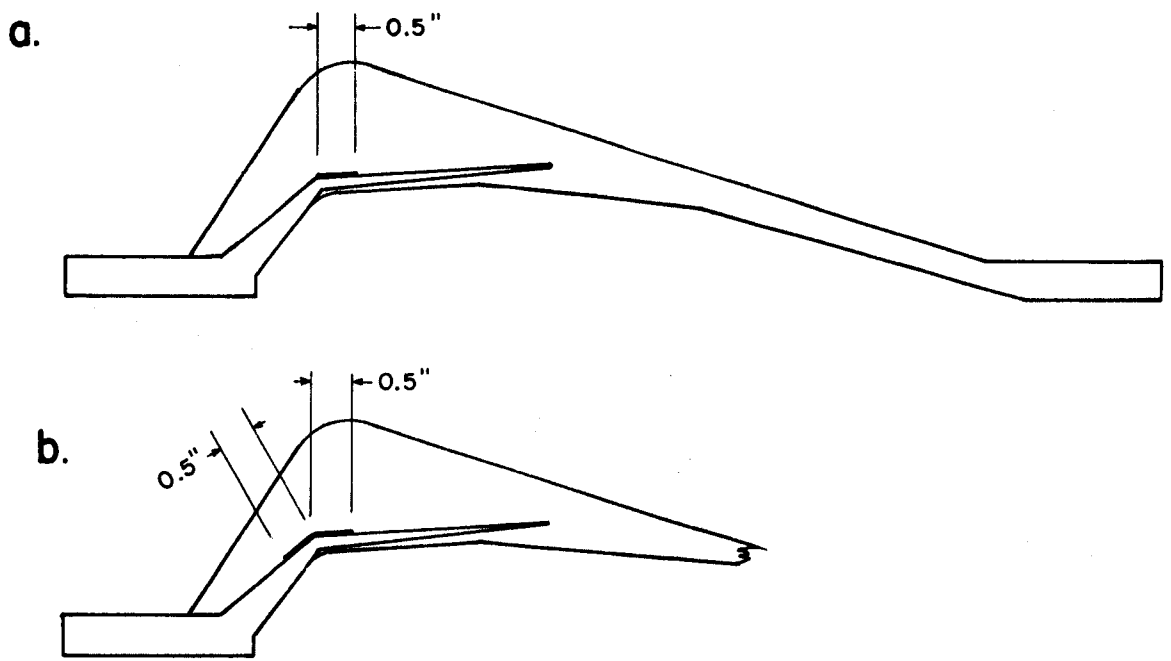


FIG. 6

STRESS CONCENTRATION MODELS

FIG. 7

# STRESS CONCENTRATIONS DUE TO SLITS

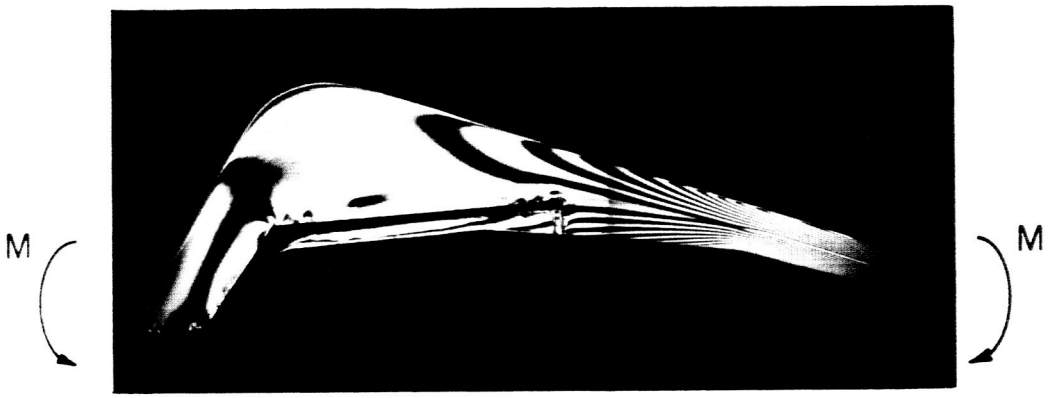


a. 0.5" LONG SLIT


b. 1.0" LONG SLIT

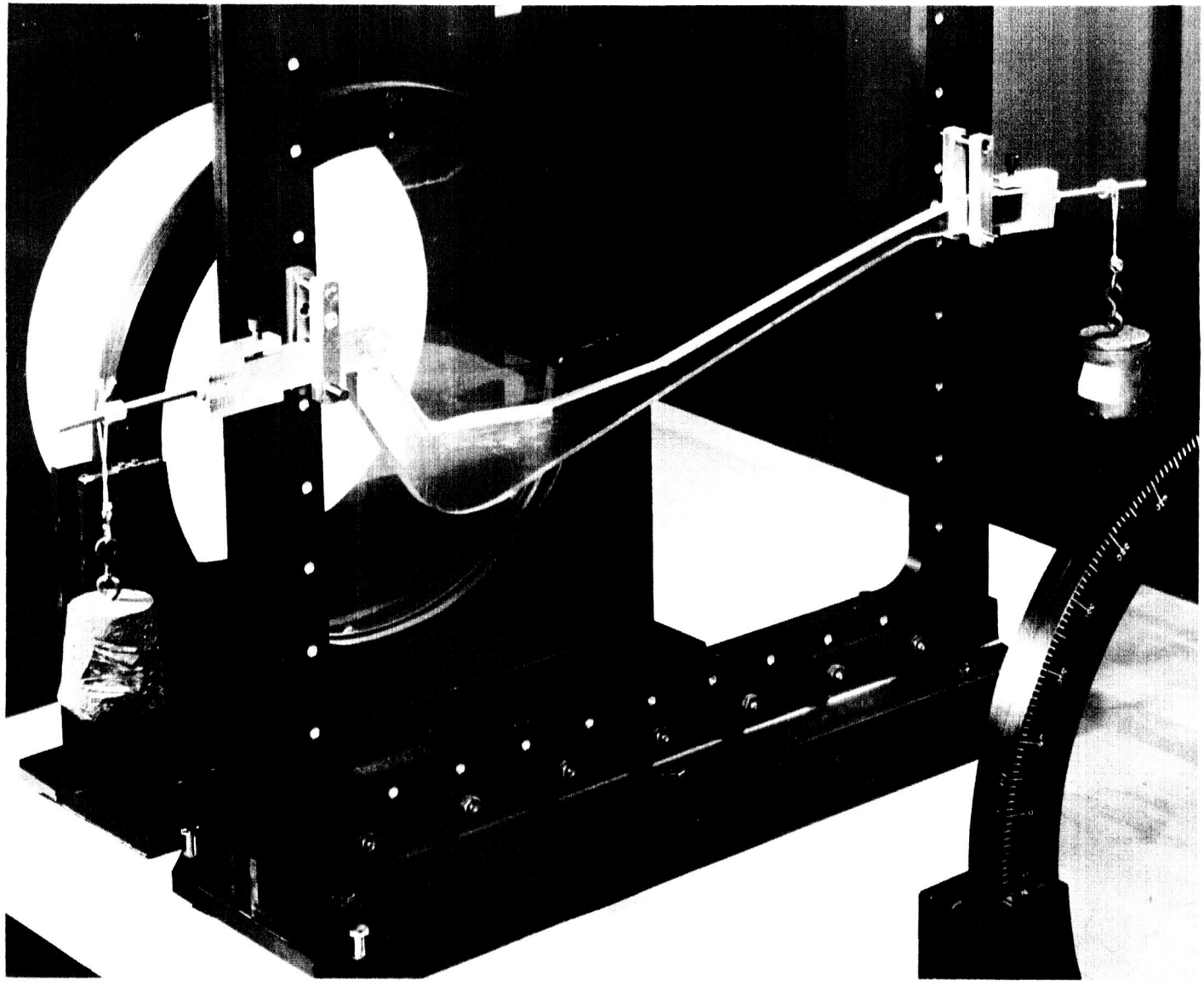

FIG. 8

TWO-DIMENSIONAL MODEL BENDING TEST

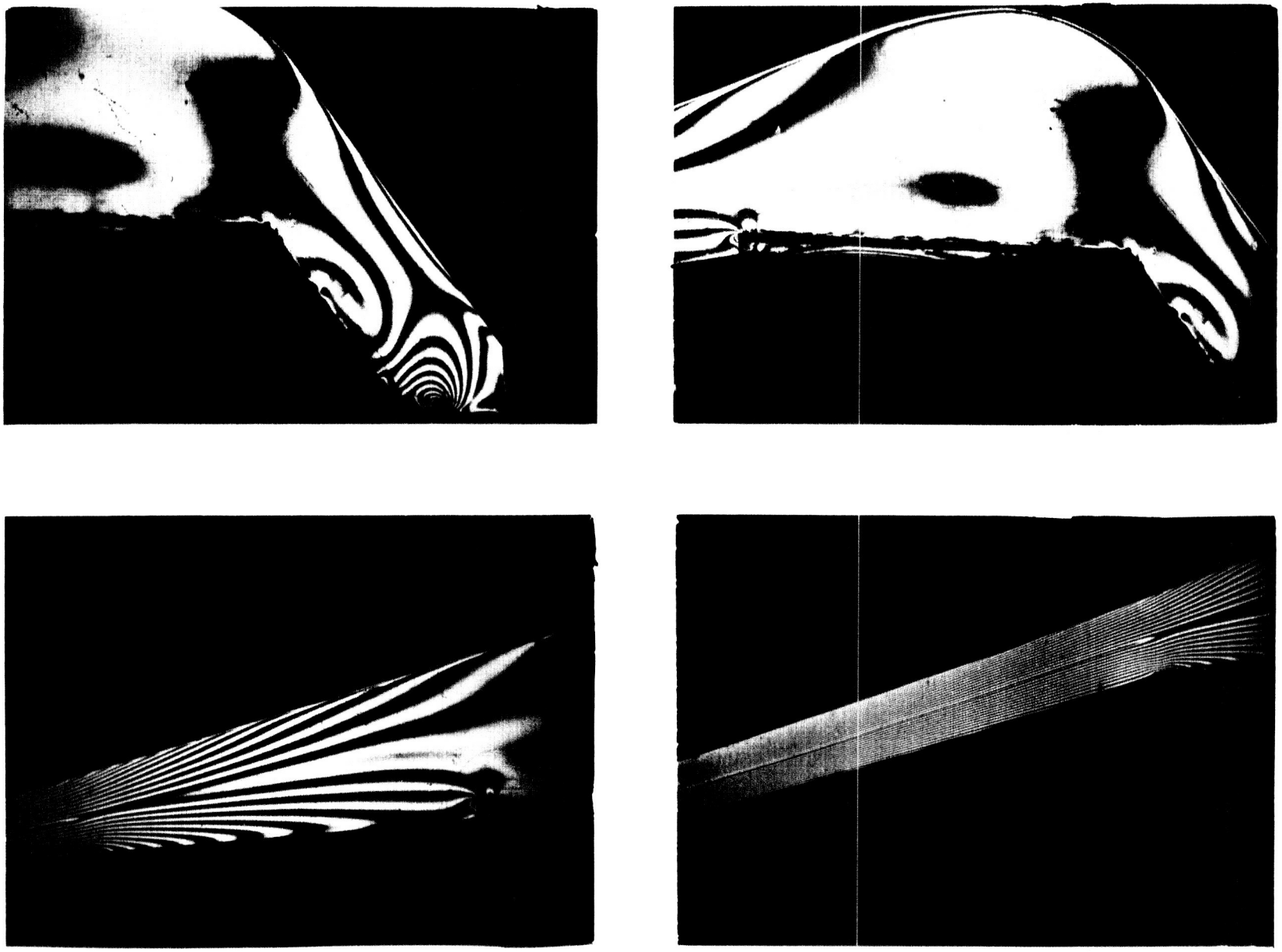

FIG. 9

ALGOL II A-55"# LOAD

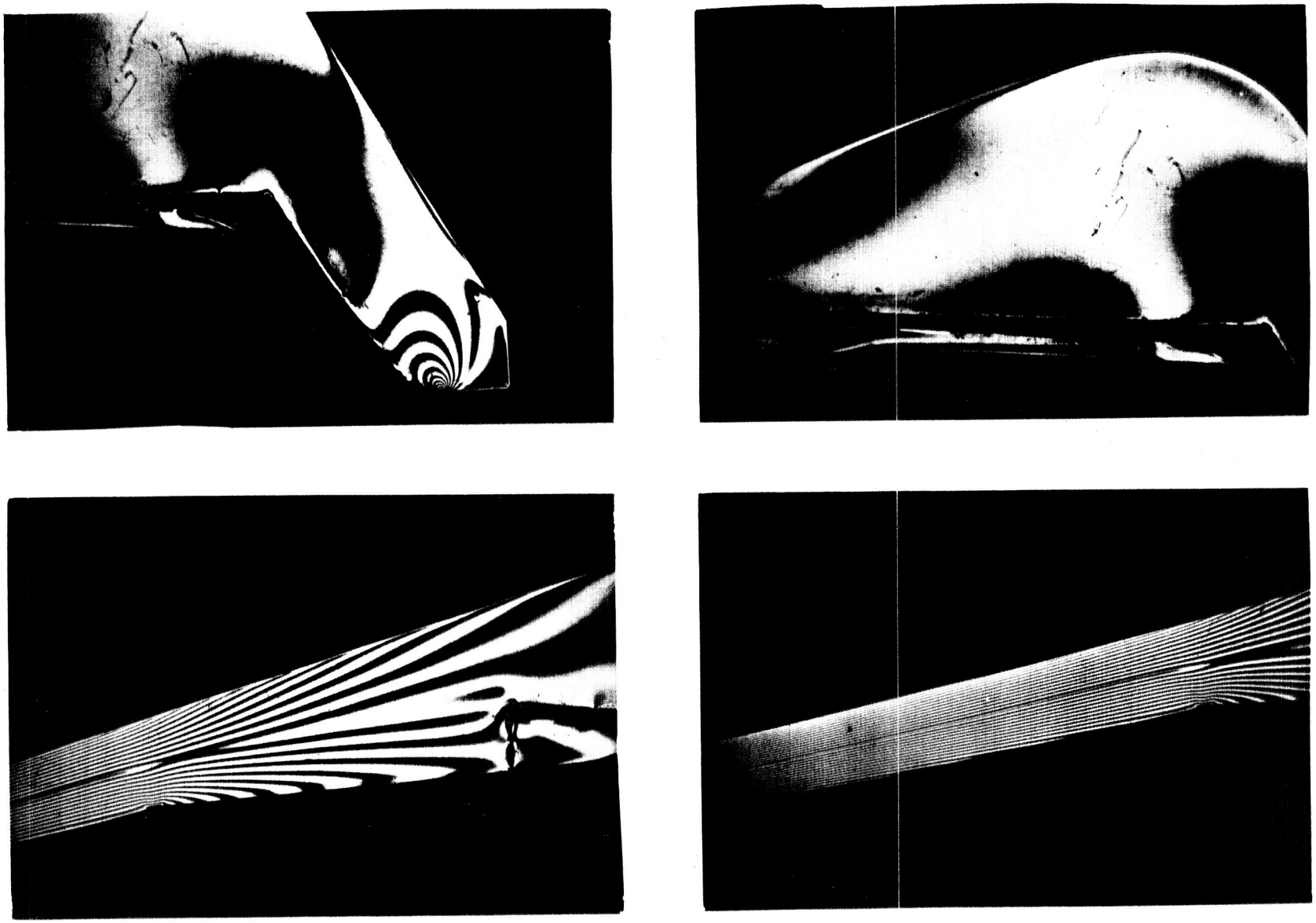

FIG. 10

ALGOL II B-55"# LOAD

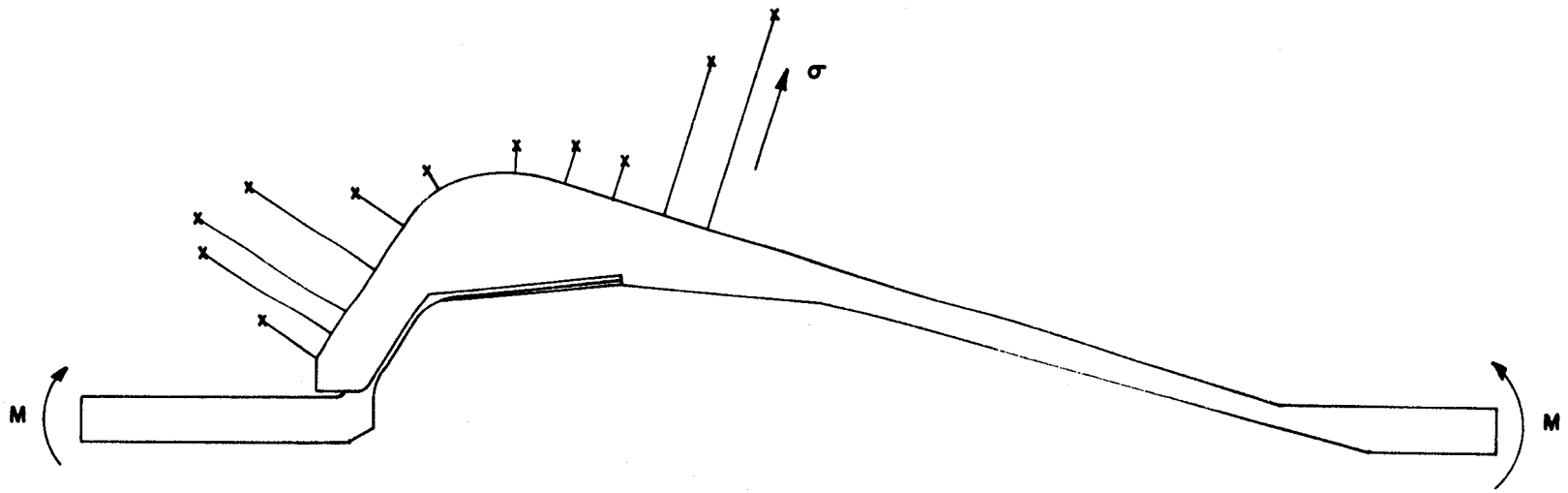


FIG. 11

## ALGOL II A
## SURFACE STRESSES AT THROAT SECTION

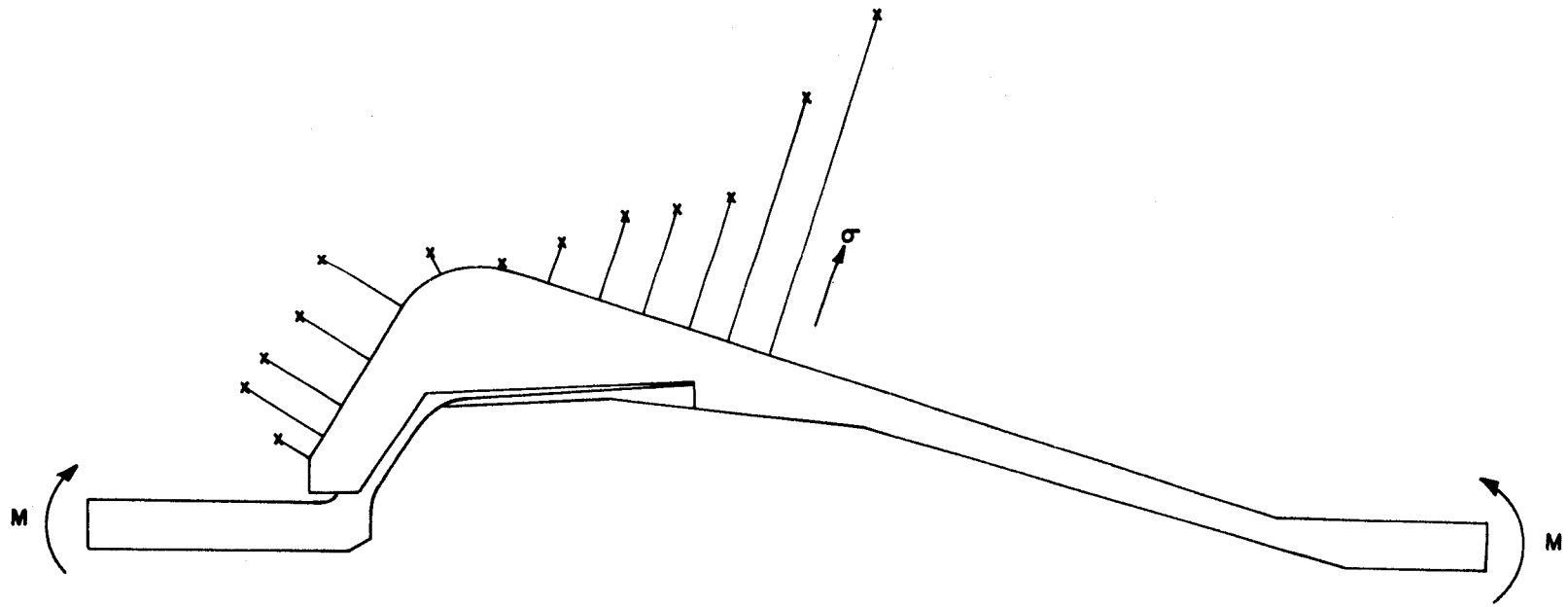


FIG. 12

ALGOL IIB
SURFACE STRESSES AT THROAT SECTION

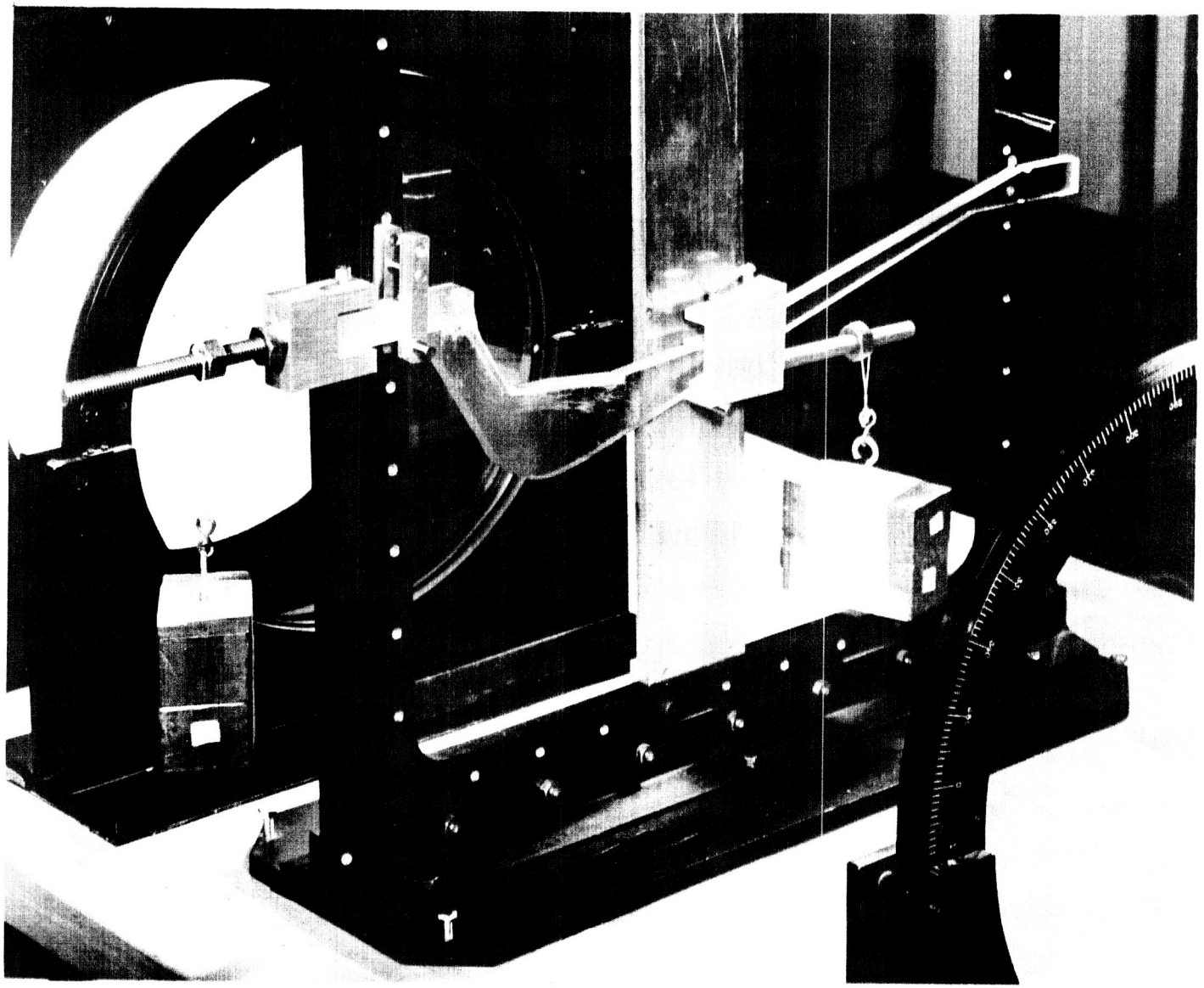

FIG. 13

APPARATUS FOR LOADING THROAT SECTION

FIG. 14

ALGOL II A-140"# LOAD

FIG. 15

ALGOL II B-140"# LOAD

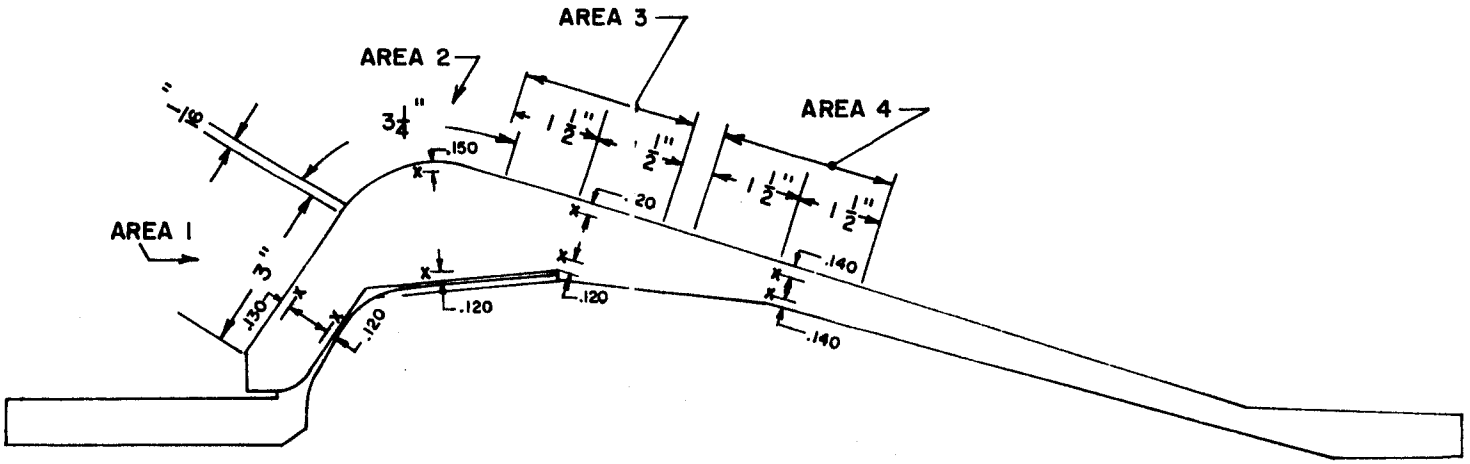


THERMOCOUPLE LOCATIONS DENOTED BY "X"

FIG. 16

# ALGOL II A

## LOCATIONS OF THERMAL STRESS TEST AREAS & THERMOCOUPLE LOCATIONS

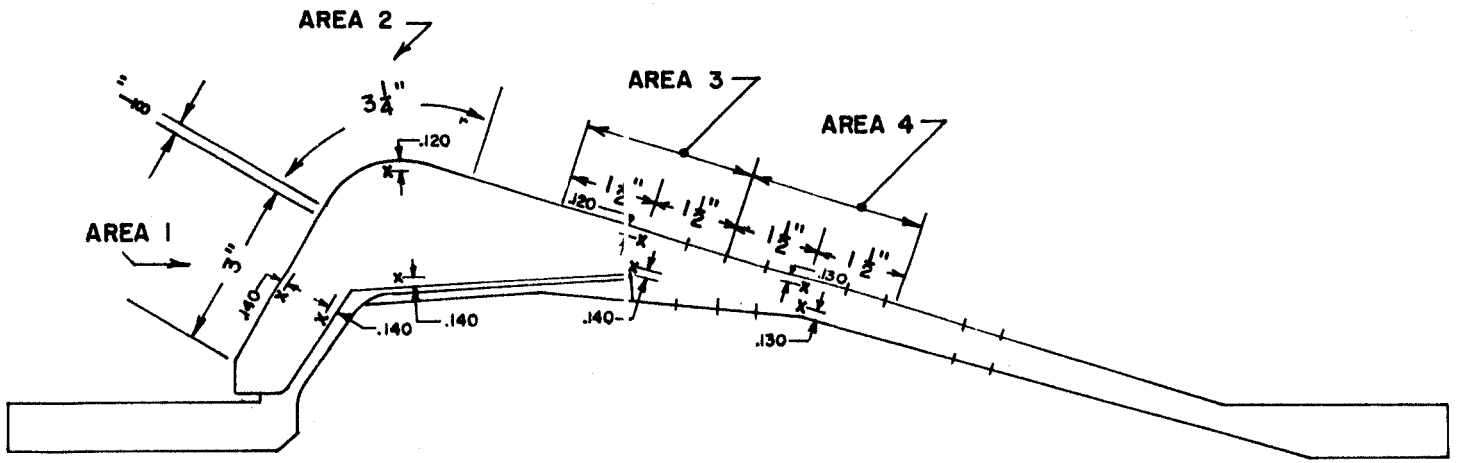


THERMOCOUPLE LOCATIONS DENOTED BY "X"

FIG. 17

# ALGOL II B
# LOCATIONS OF THERMAL STRESS TEST AREAS & THERMOCOUPLE LOCATIONS

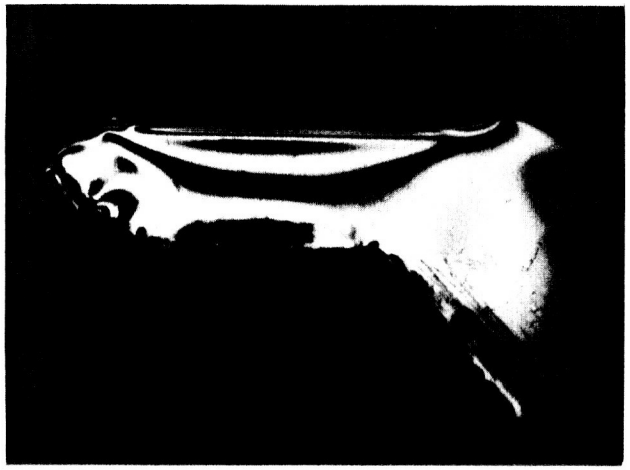

t=30 SEC.

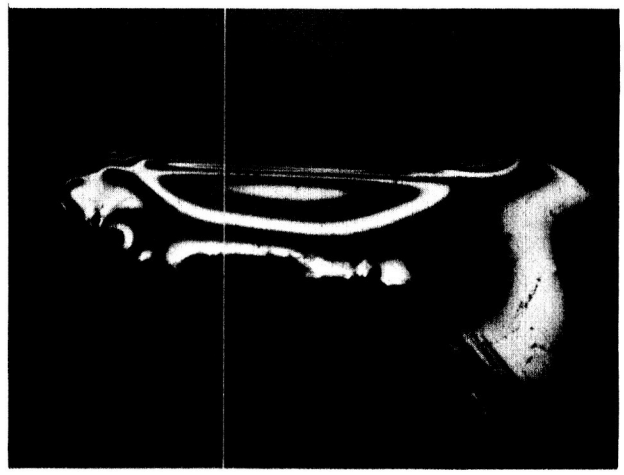

t=1 MIN.

t=2 MIN.

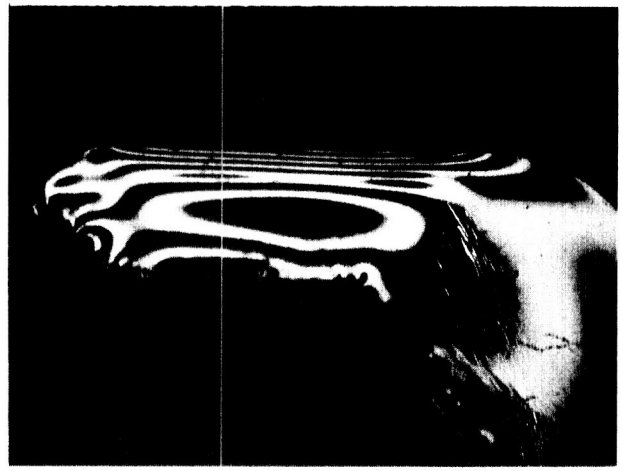

t=4 MIN.

FIG. 18

ALGOL II A NOZZLE
THERMAL INDUCED STRESS-AREA # 1

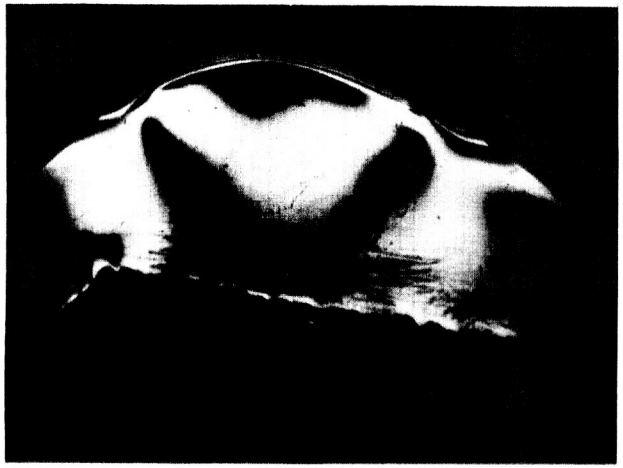

t = 30 SEC.

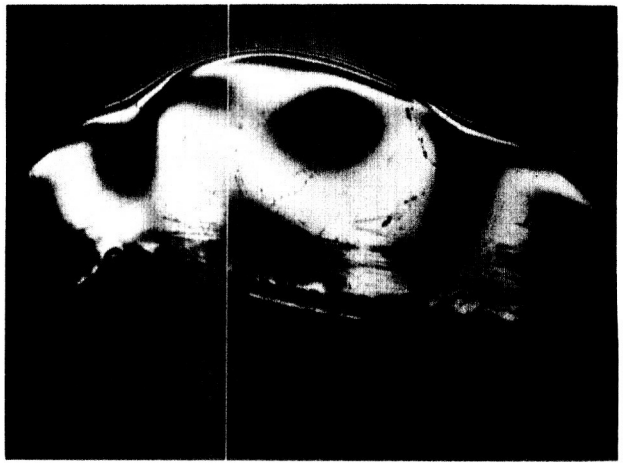

t = 1 MIN.

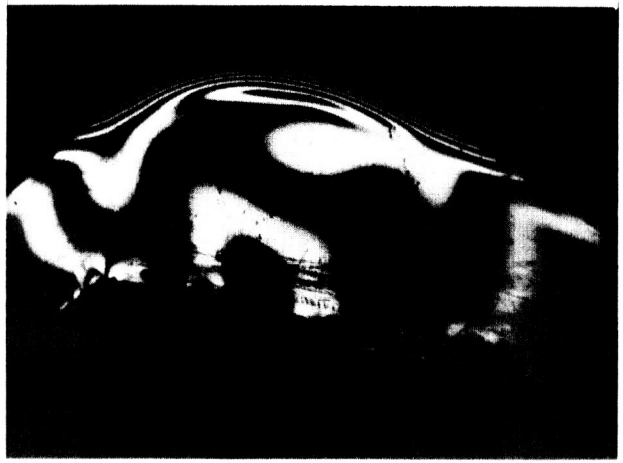

t = 2 MIN

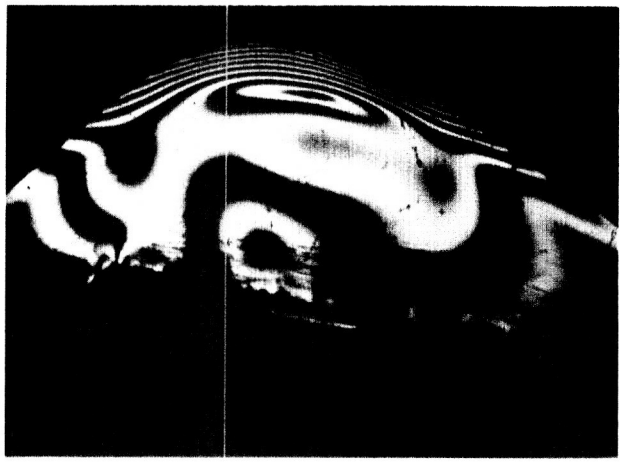

t = 4 MIN

FIG. 19

ALGOL II A NOZZLE
THERMAL INDUCED STRESS–AREA # 2

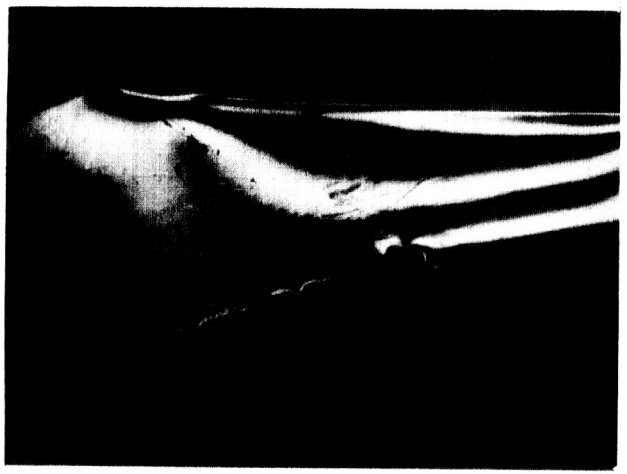

t=30 SEC.

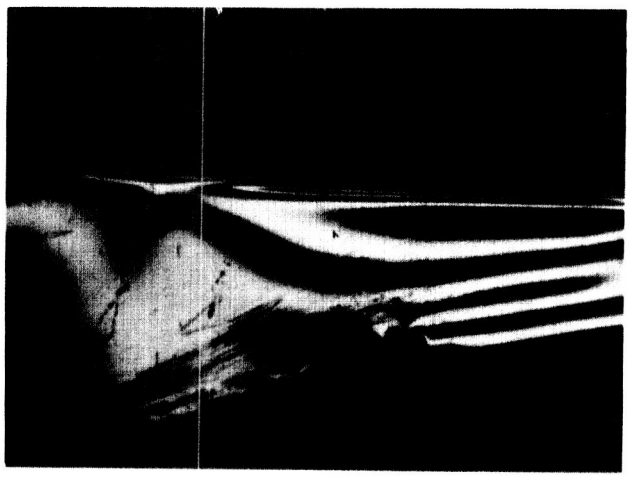

t=1 MIN.

t=2 MIN.

t=4 MIN.

FIG. 20

ALGOL II A NOZZLE
THERMAL INDUCED STRESS–AREA # 3

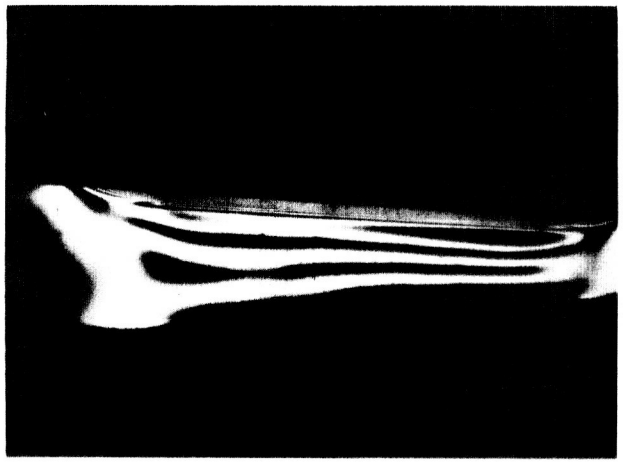

t = 30 SEC.

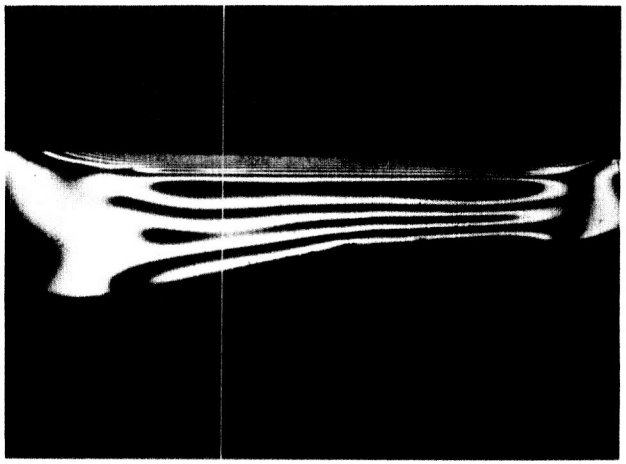

t = 1 MIN.

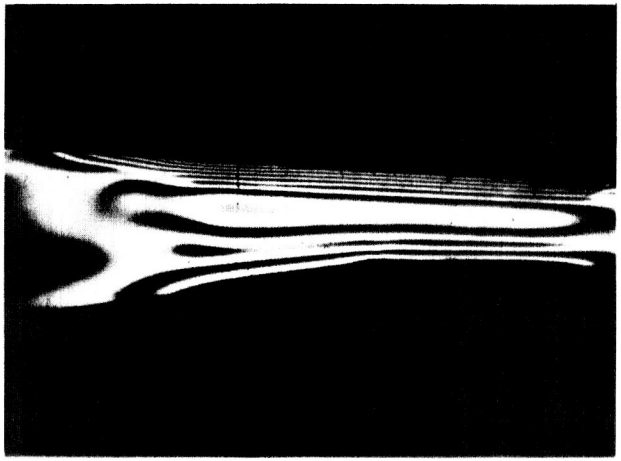

t = 2 MIN.

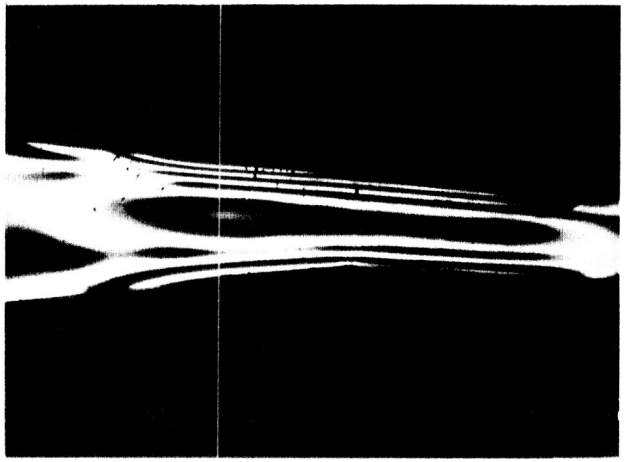

t = 4 MIN.

FIG. 21

ALGOL IIA NOZZLE
THERMAL INDUCED STRESS–AREA #4

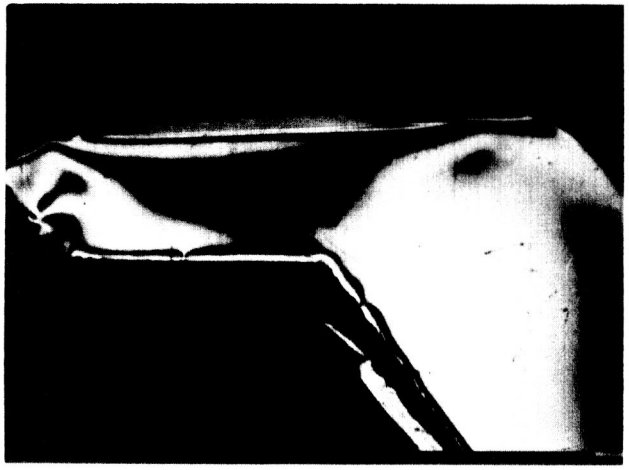

t=30 SEC

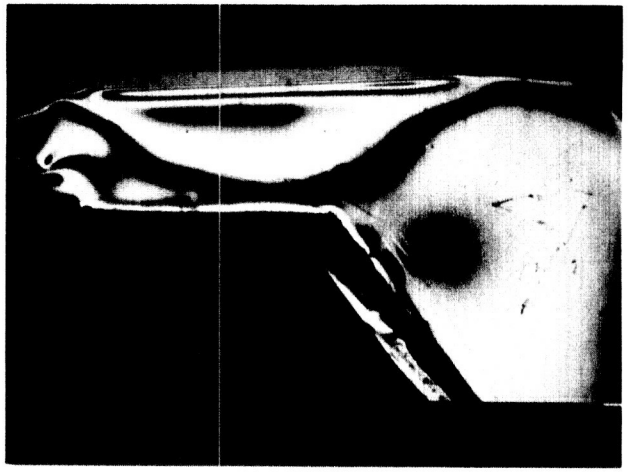

t=1 MIN.



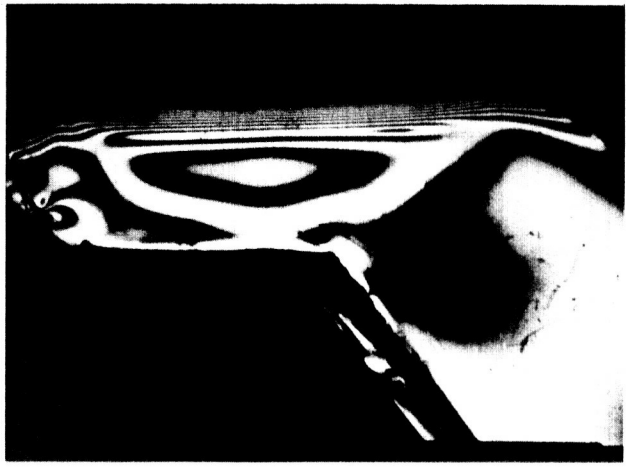

t=2 MIN.

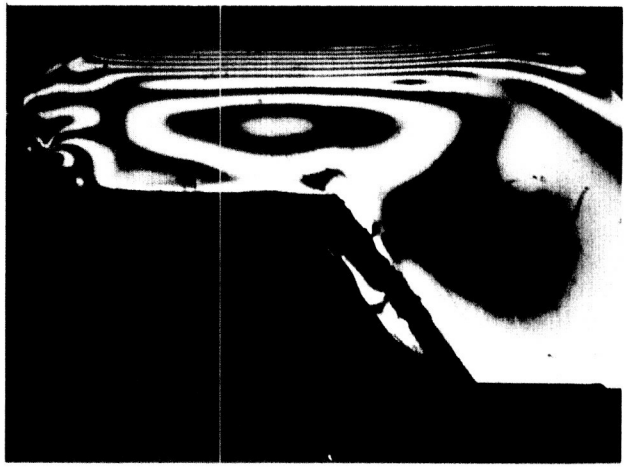

t=4 MIN.

FIG. 22

ALGOL IIB NOZZLE
THERMAL INDUCED STRESS-AREA #1

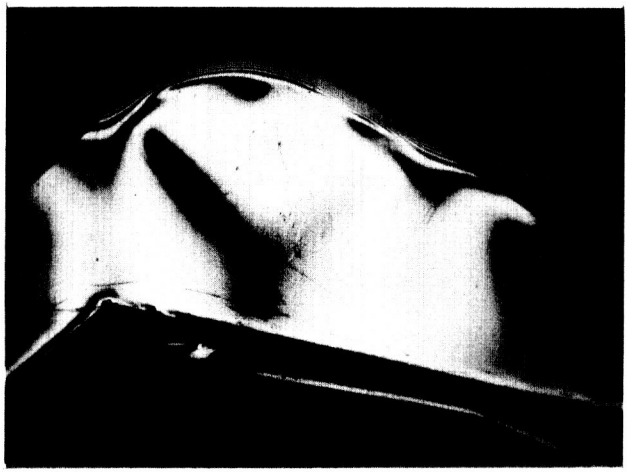

t=30 SEC.

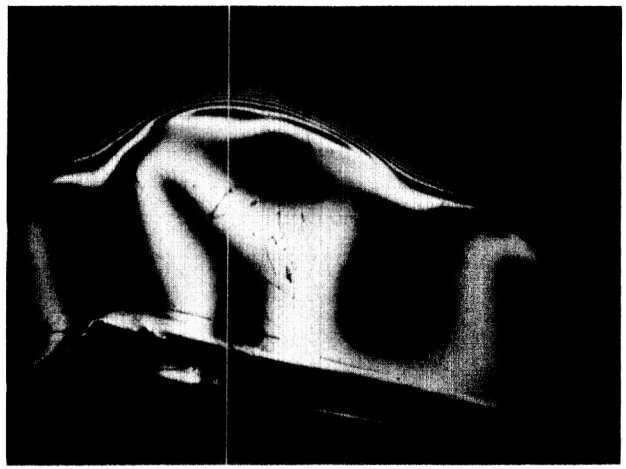

t=1 MIN.

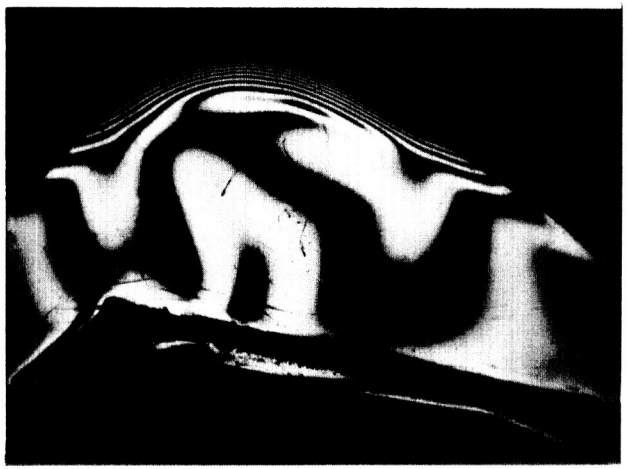

t=2 MIN.

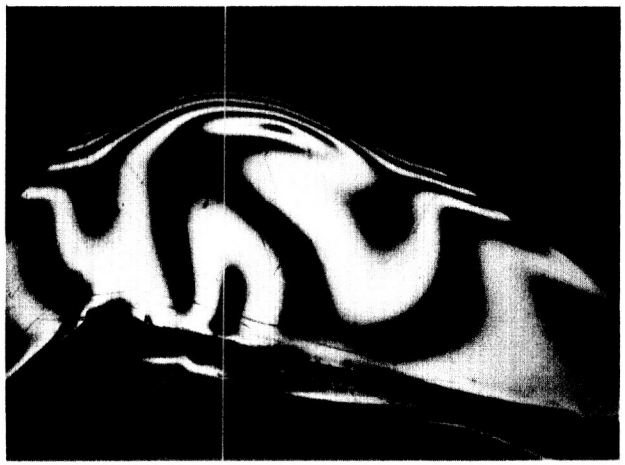

t=4 MIN.

FIG. 23

ALGOL II B NOZZLE
THERMAL INDUCED STRESS—AREA #2

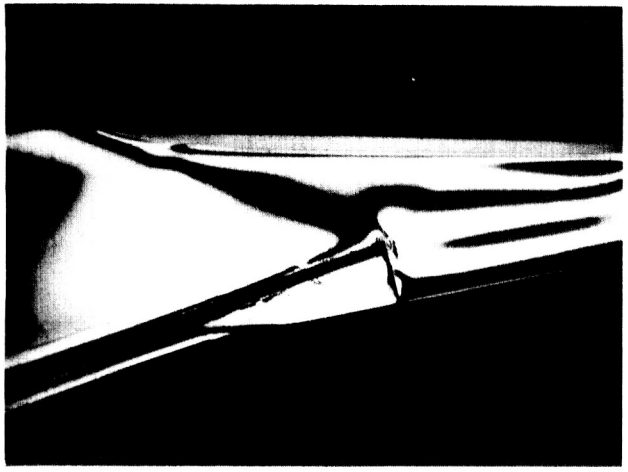

t = 30 SEC.

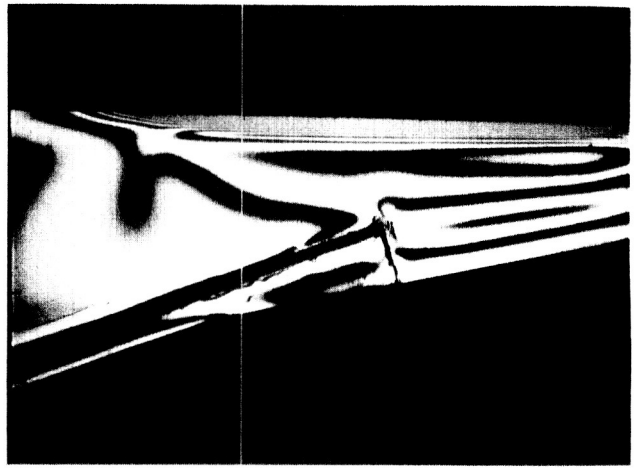

t = 1 MIN.



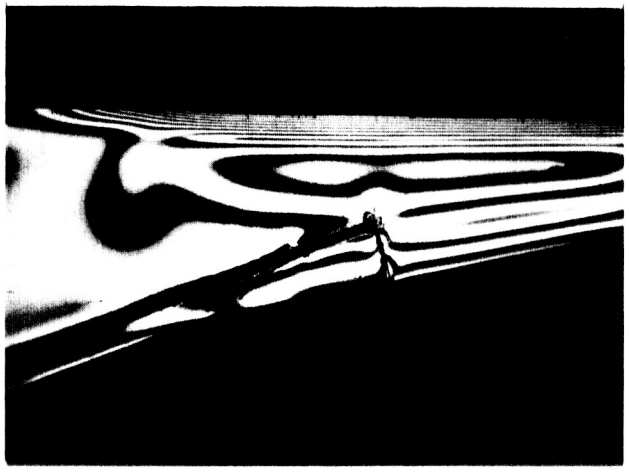

t = 2 MIN.

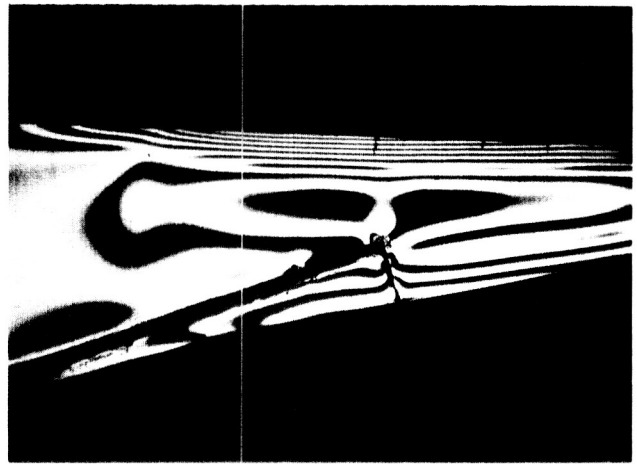

t = 4 MIN.

FIG. 24

ALGOL IIB NOZZLE
THERMAL INDUCED STRESS—AREA #3

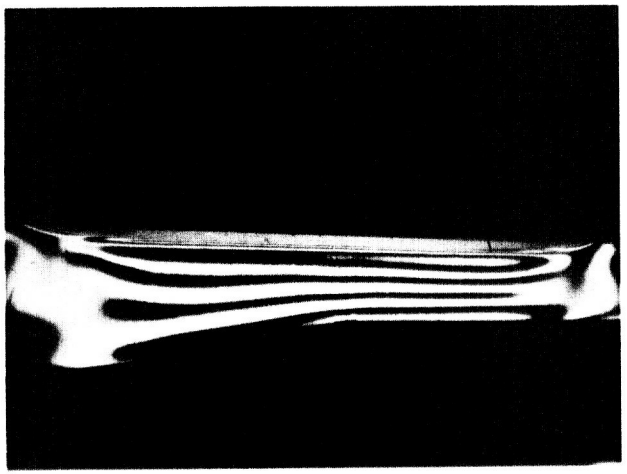

t=30 SEC.

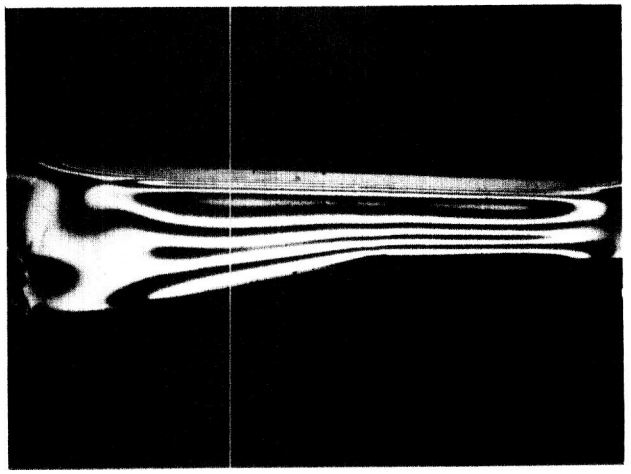

t=1 MIN.

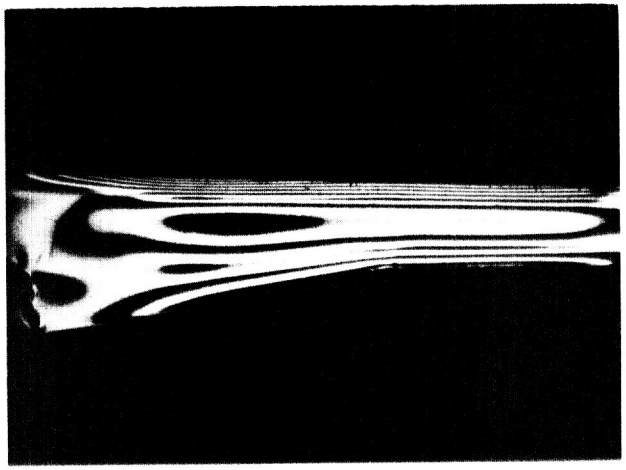

t=2 MIN.

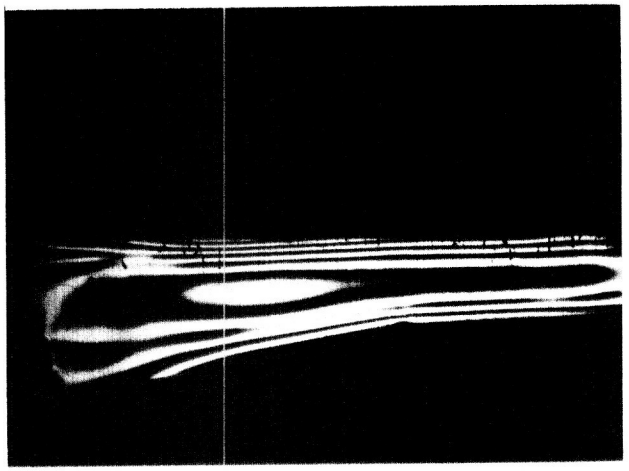

t=4 MIN.

FIG. 25

ALGOL II B NOZZLE
THERMAL INDUCED STRESS—AREA #4

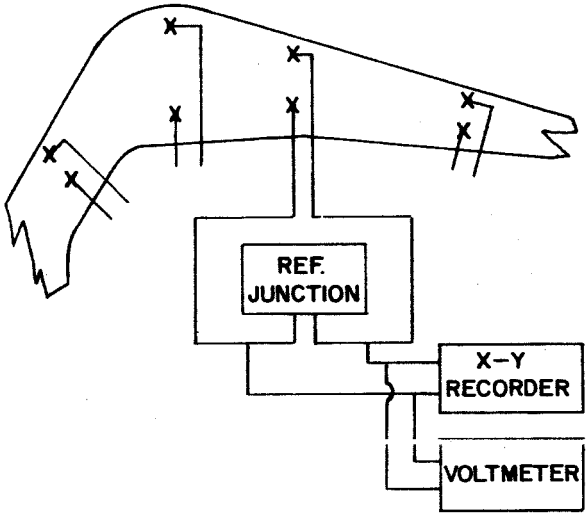


FIG. 26

# BLOCK DIAGRAM OF THERMOCOUPLE MEASUREMENT SETUP ON THERMAL STRESS TESTS

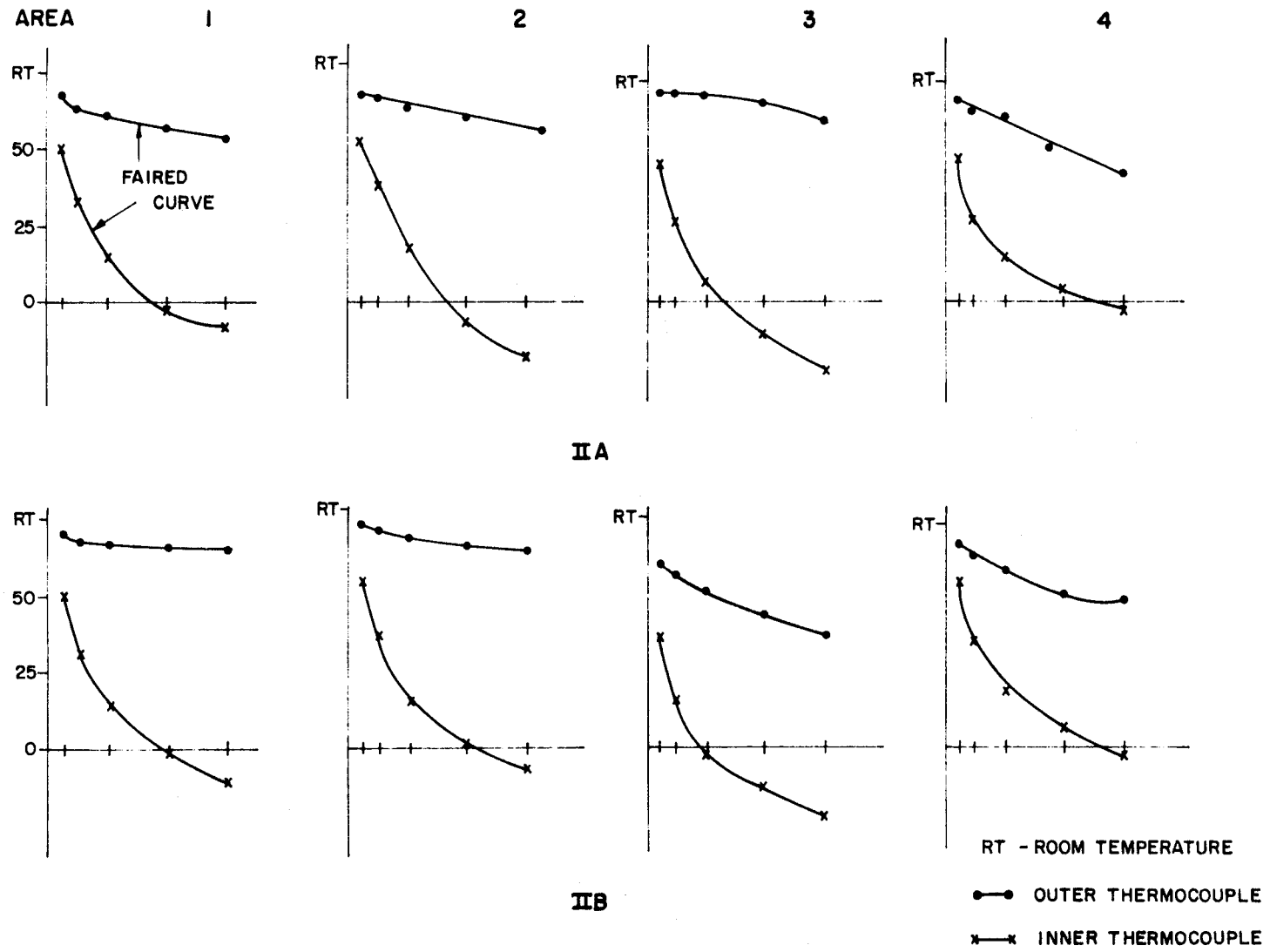


FIG. 27

# TEMPERATURE PROFILES FROM THERMAL GRADIENT TESTS

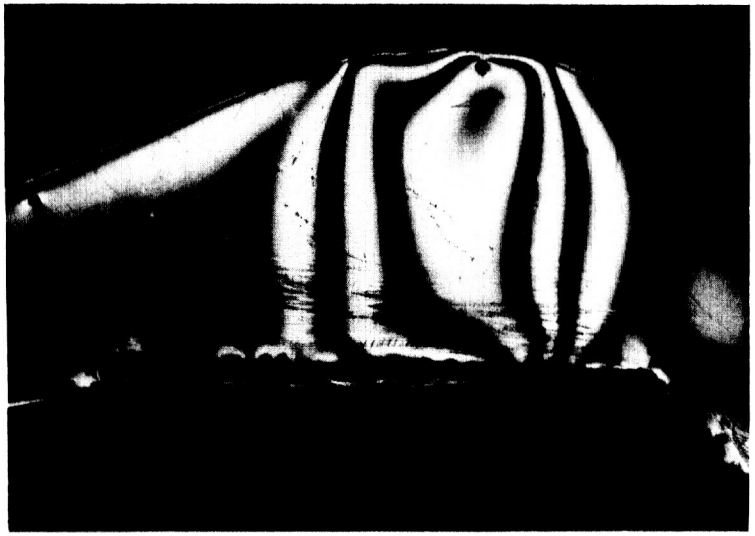

ALGOL II A

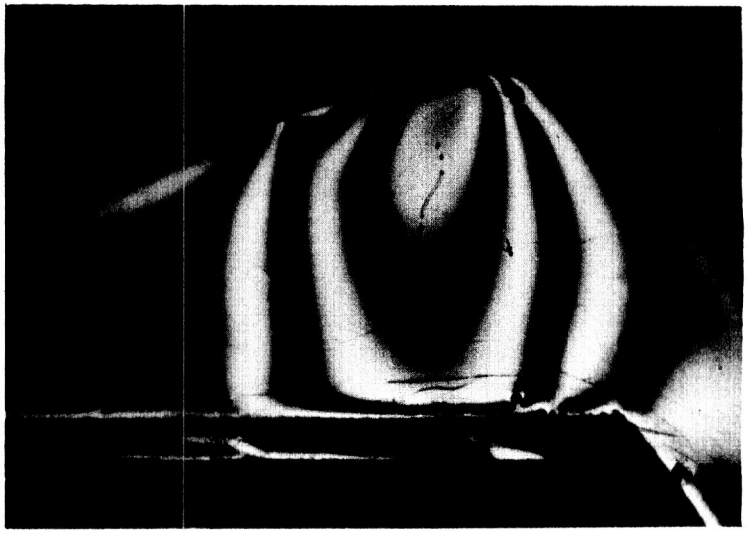

ALGOL II B

FIG. 28

PRESSURE LOADING THROAT SECTION

ALGOL II A

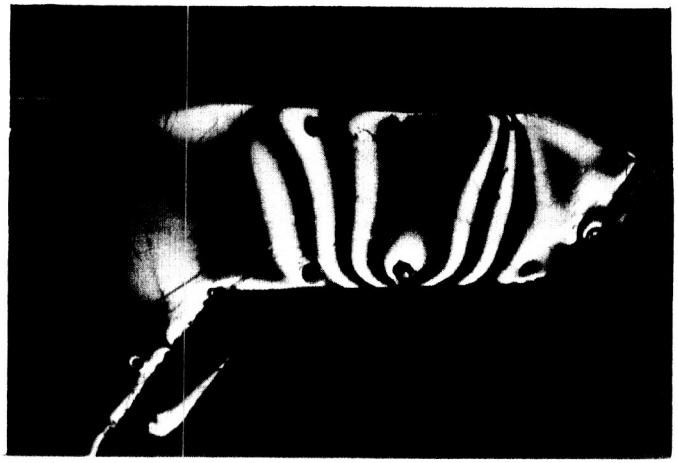

ALGOL II B

FIG. 29

PRESSURE LOADING ENTRANCE SECTION

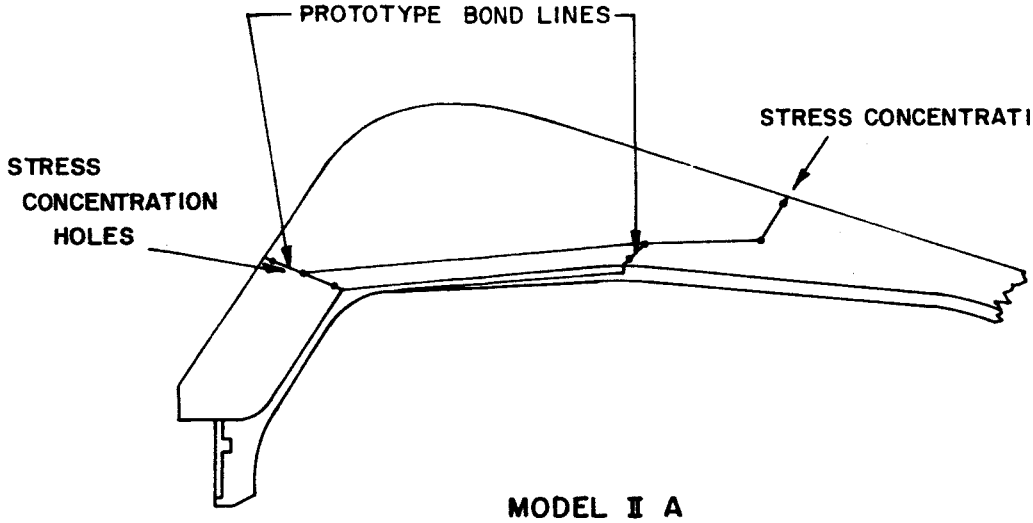


MODEL II A

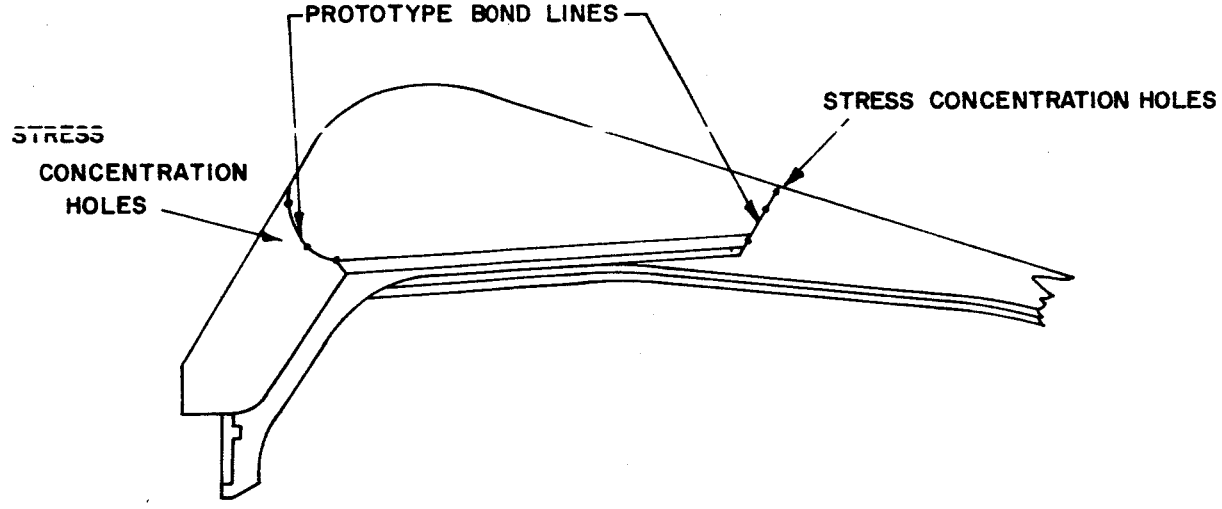


MODEL II B

FIG. 30

# LOCATION OF STRESS CONCENTRATION HOLES

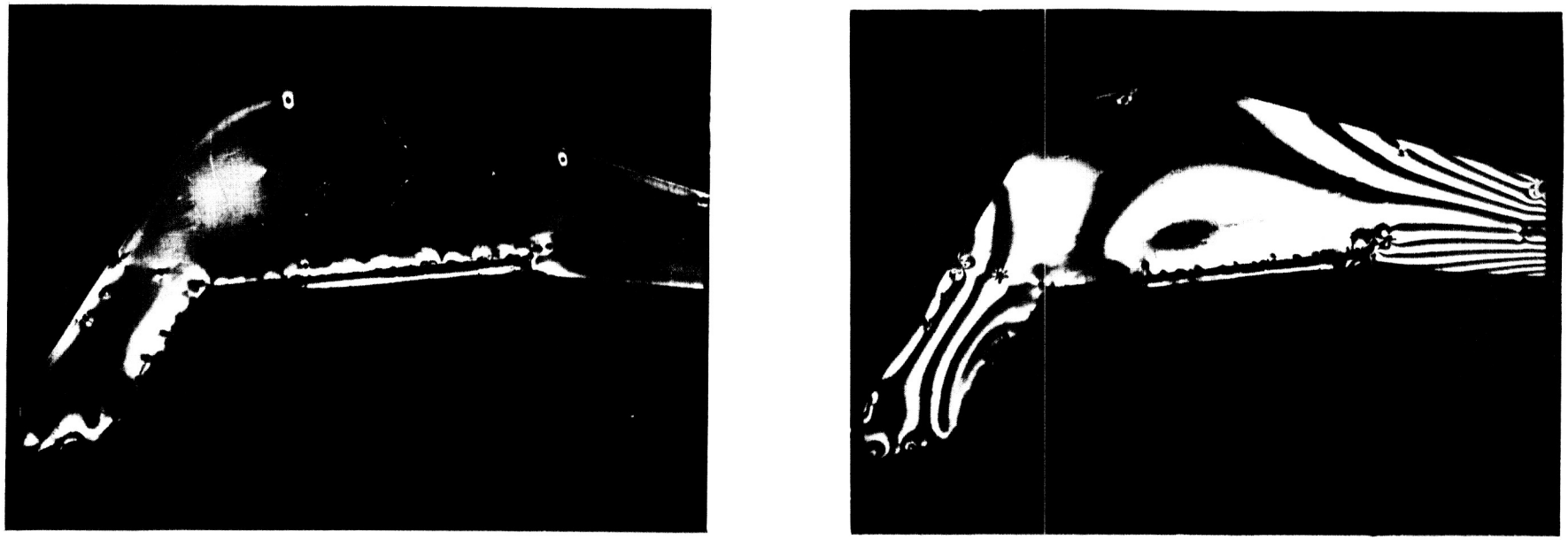

FIG. 31

ALGOL II A-STRESS CONCENTRATIONS

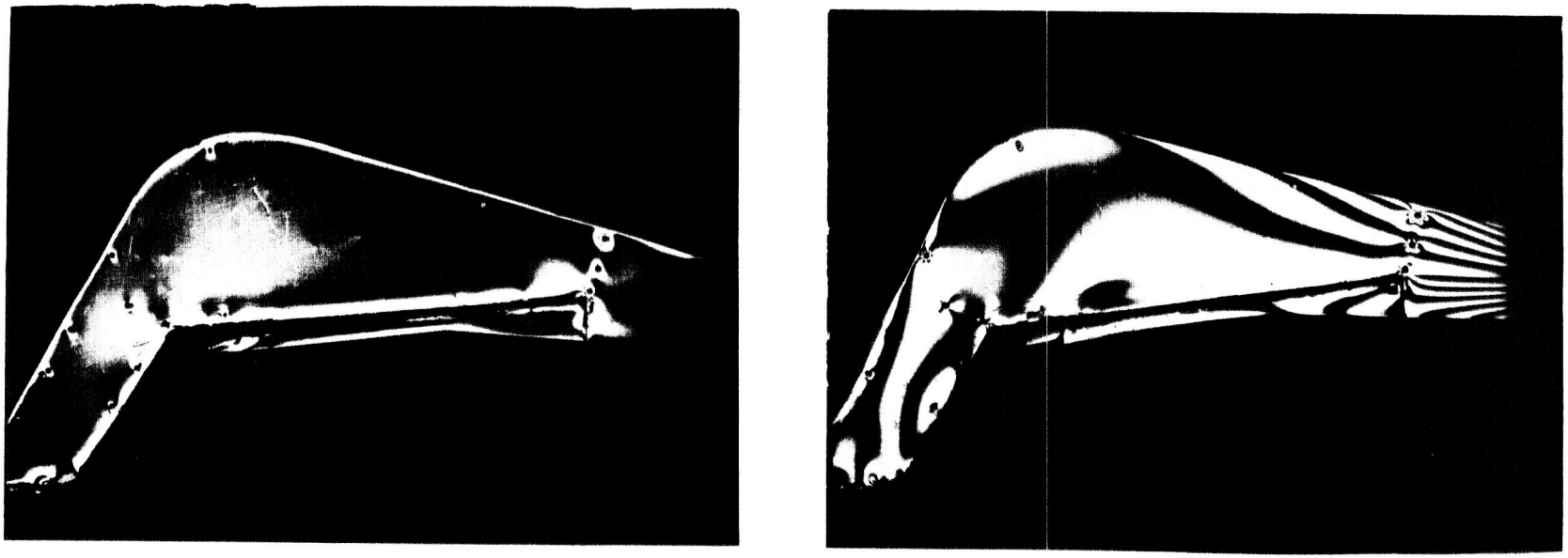

FIG. 32

ALGOL II B STRESS CONCENTRATIONS

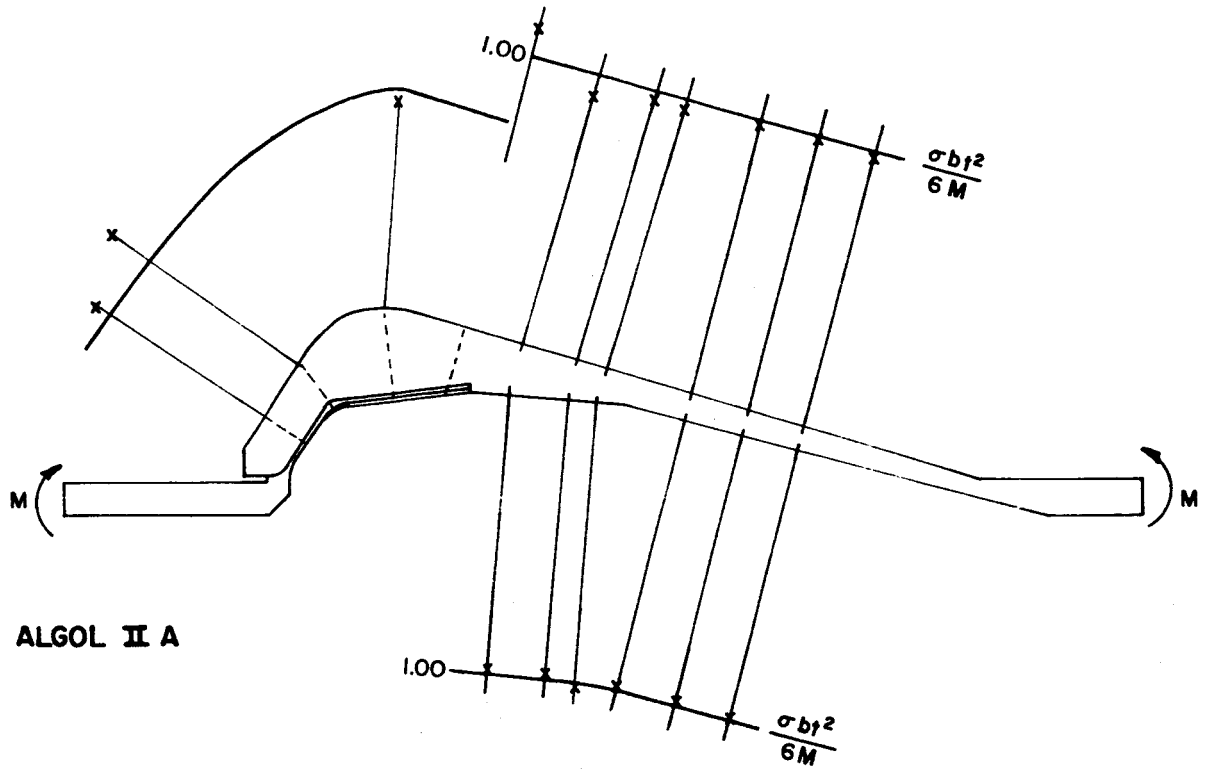


ALGOL II A

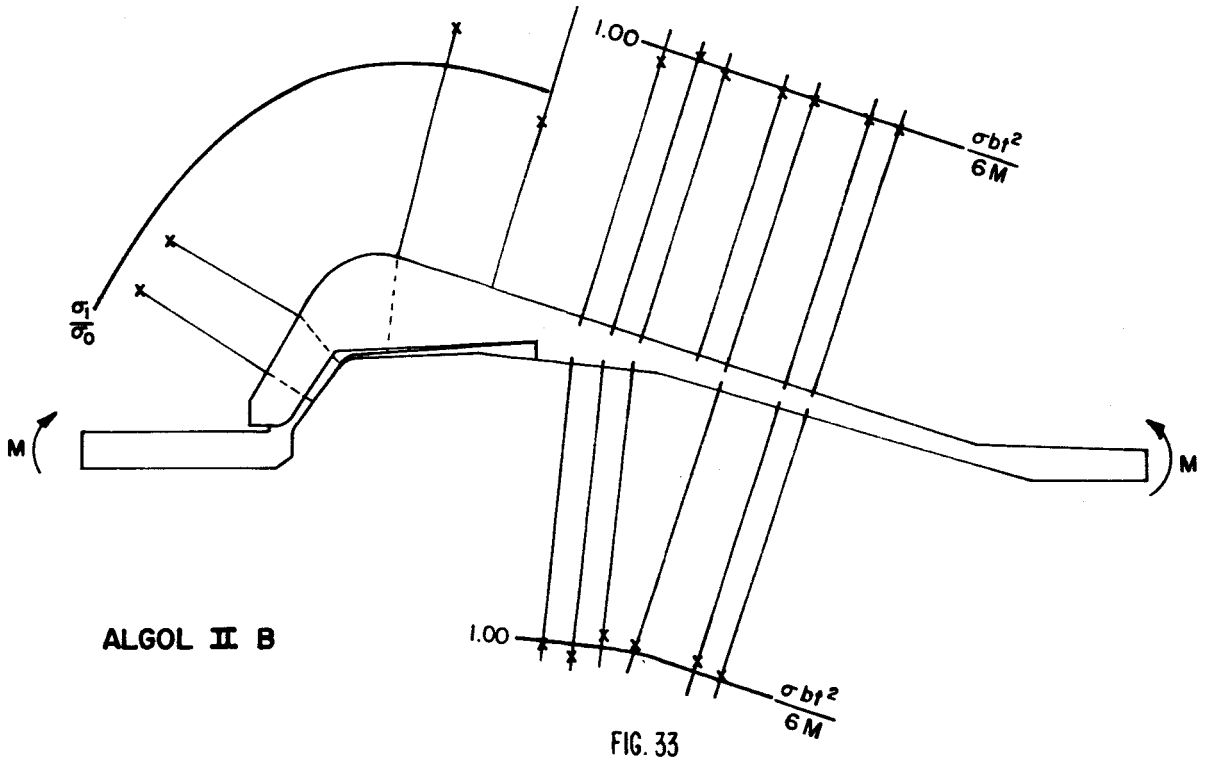


ALGOL II B

FIG. 33

# COMPARISON OF EXPERIMENTAL AND ANALYTICAL DATA FOR BENDING TESTS

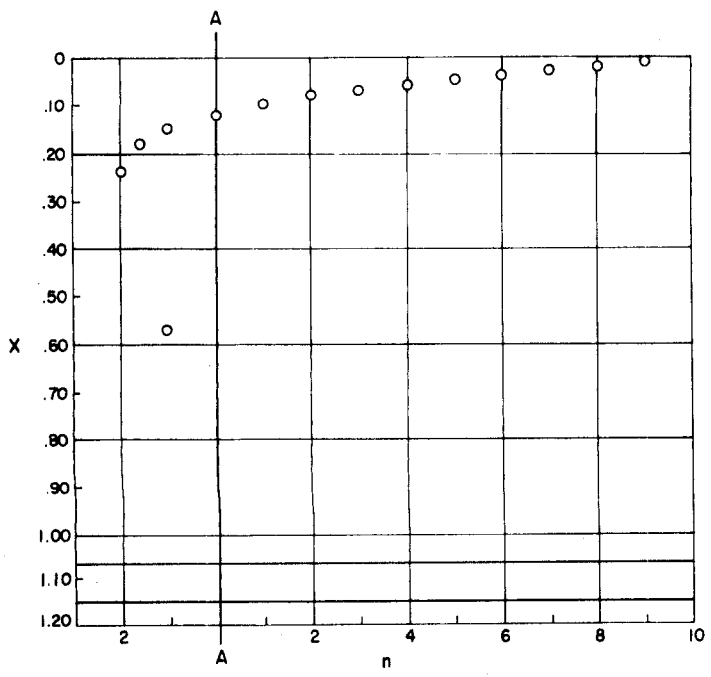


FRINGE ORDER

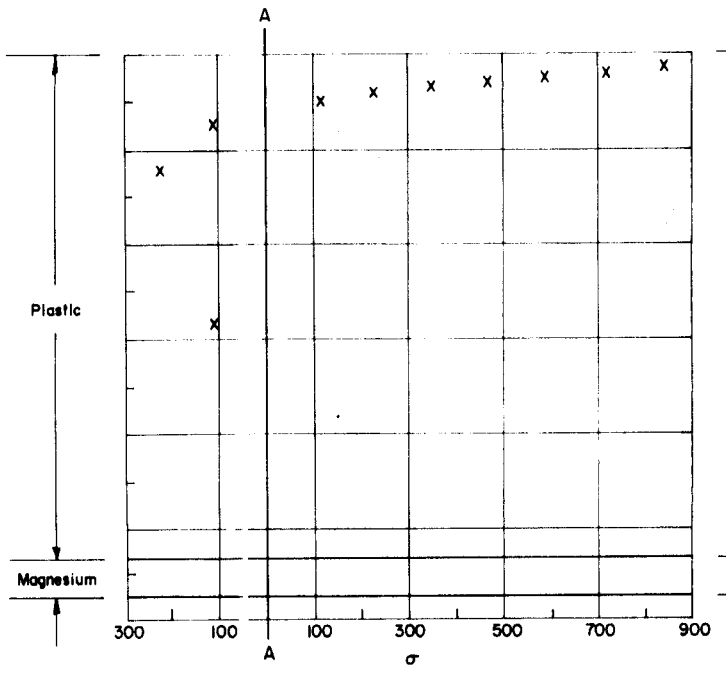


THERMAL STRESS

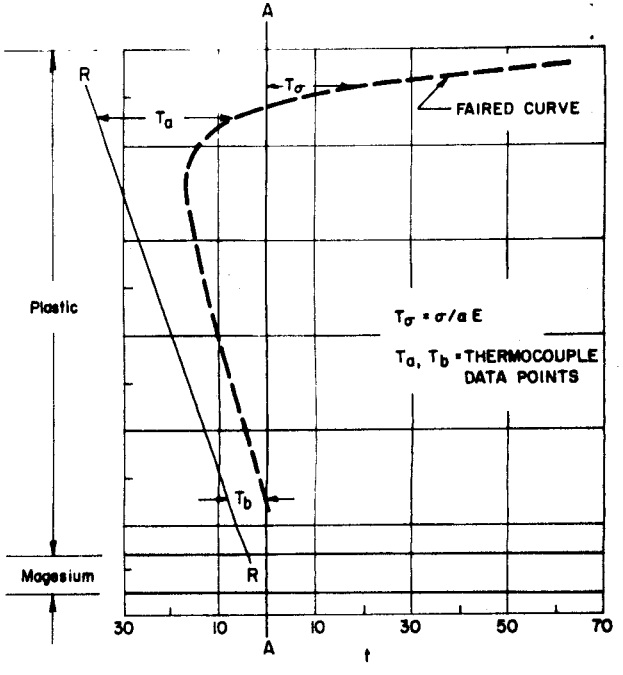


TEMPERATURE CORRESPONDING TO THERMAL STRESS

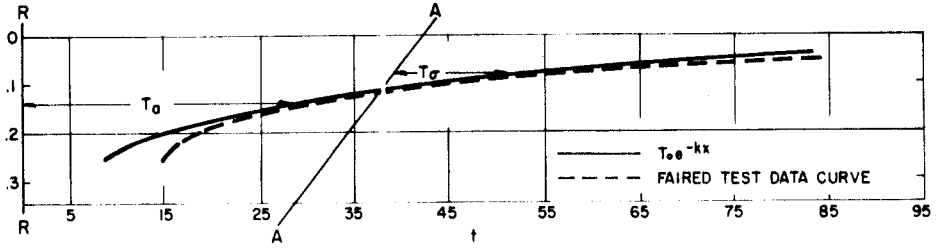


ACTUAL TEMPERATURE DISTRIBUTION IN THE THERMAL SHOCK LAYER

FIG. 34

# THERMAL TESTS-COMPARISON OF ANALYTICAL & EXPERIMENTAL DATA

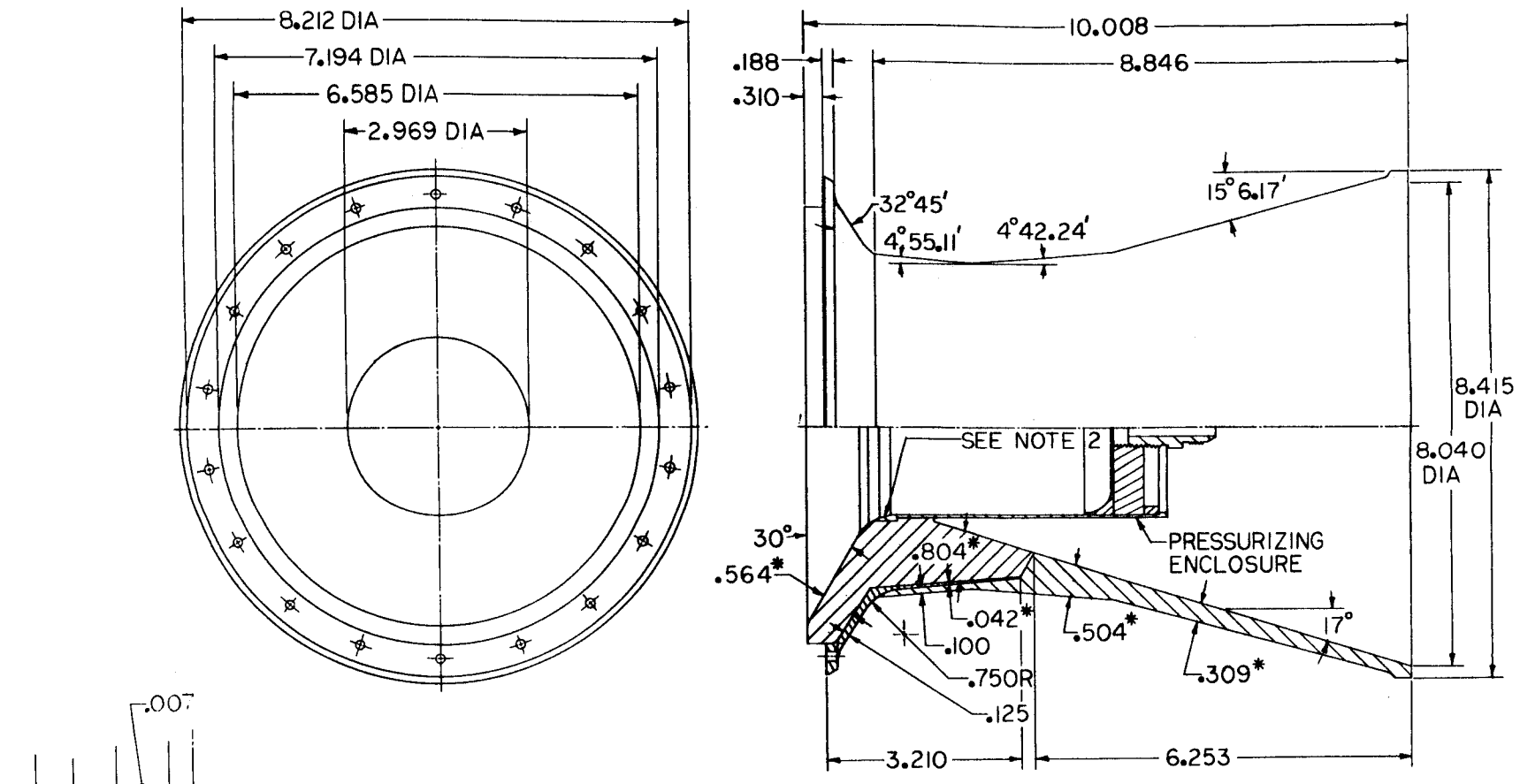


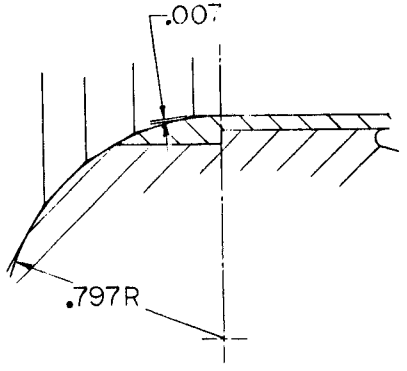


DETAIL "A"

NOTES:

1. BECAUSE OF TAPER OF SECTIONS, A DIMENSION MARKED WITH * IS AN AVERAGE THICKNESS.

2. FLATS ARE USED TO SIMULATE A RADIUS.

FIG. 15

# THREE-DIMENSIONAL MODEL WITH PRESSURE CLOSURE IN THROAT

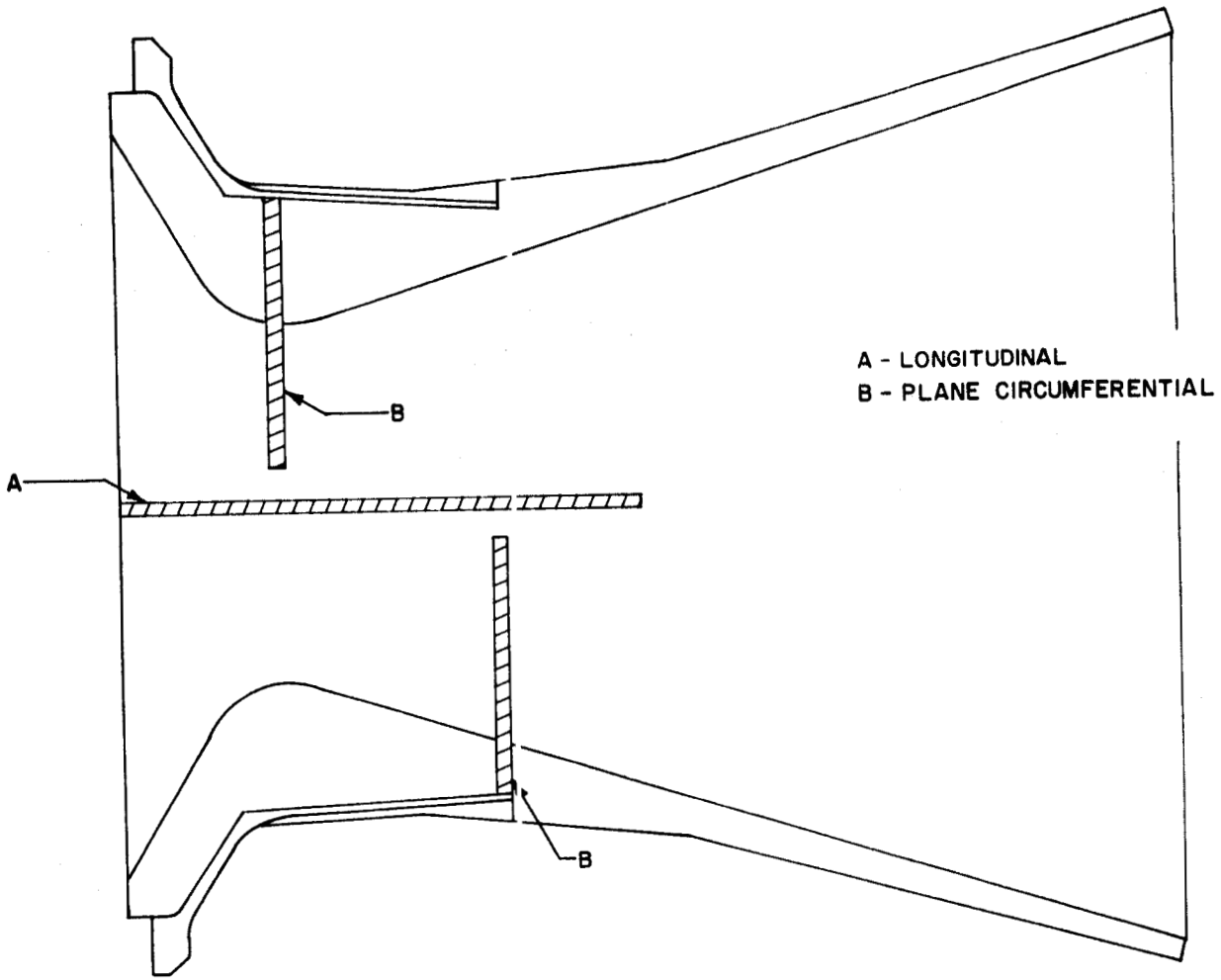


FIG. 36

ALGOL IIB NOZZLE
LOCATION OF BONDED POLARISCOPES

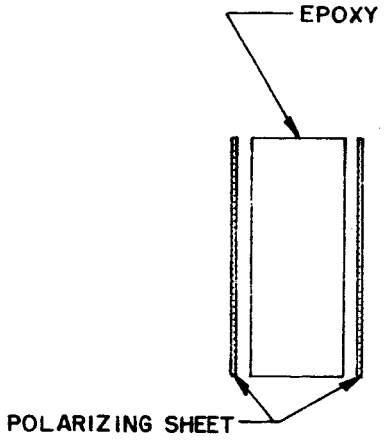


CIRCUMFERENTIAL

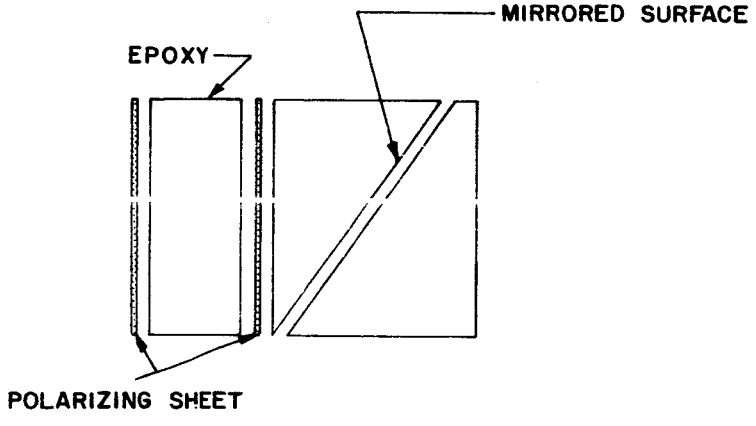


LONGITUDINAL

FIG. 37

# BONDED POLARISCOPE SUB-ASSEMBLIES

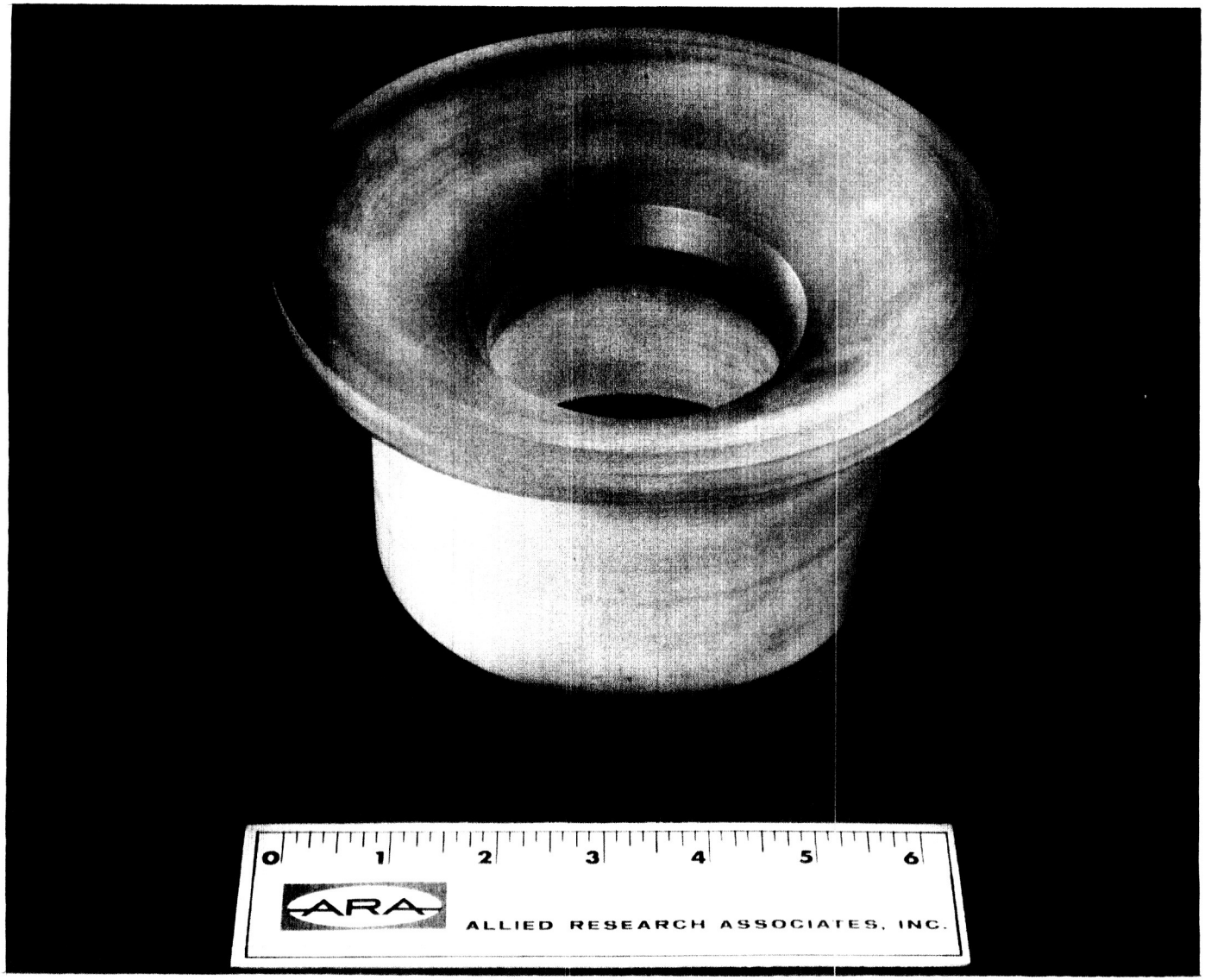


FIG. 38

BLANK FOR THROAT SECTION

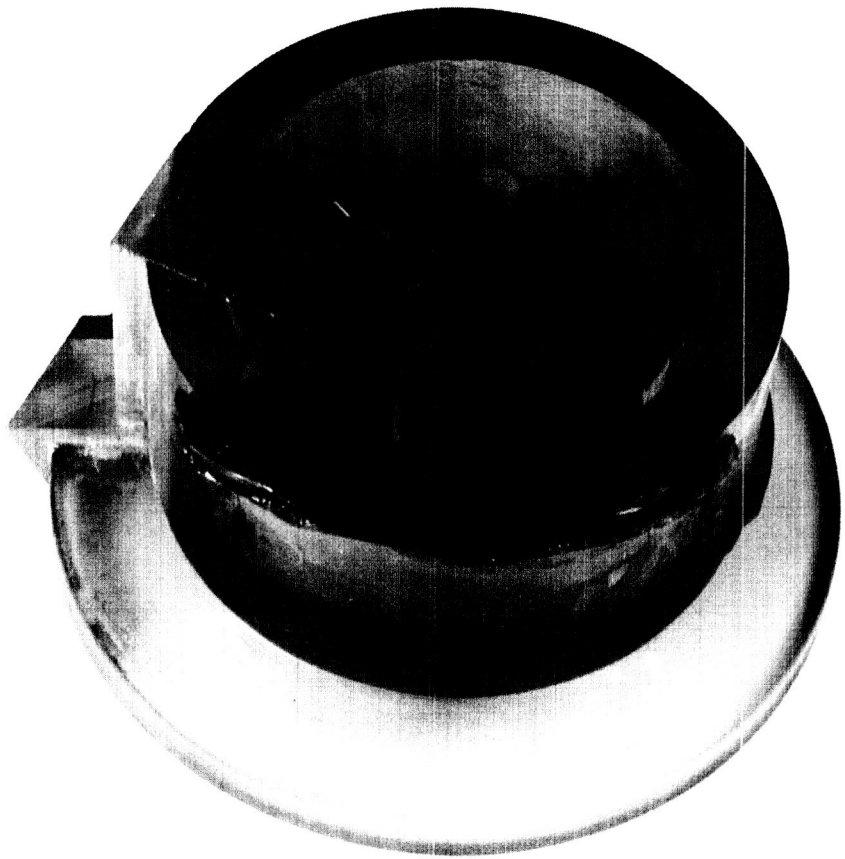

FIG. 39

BLANK WITH POLARISCOPES BONDED IN PLACE

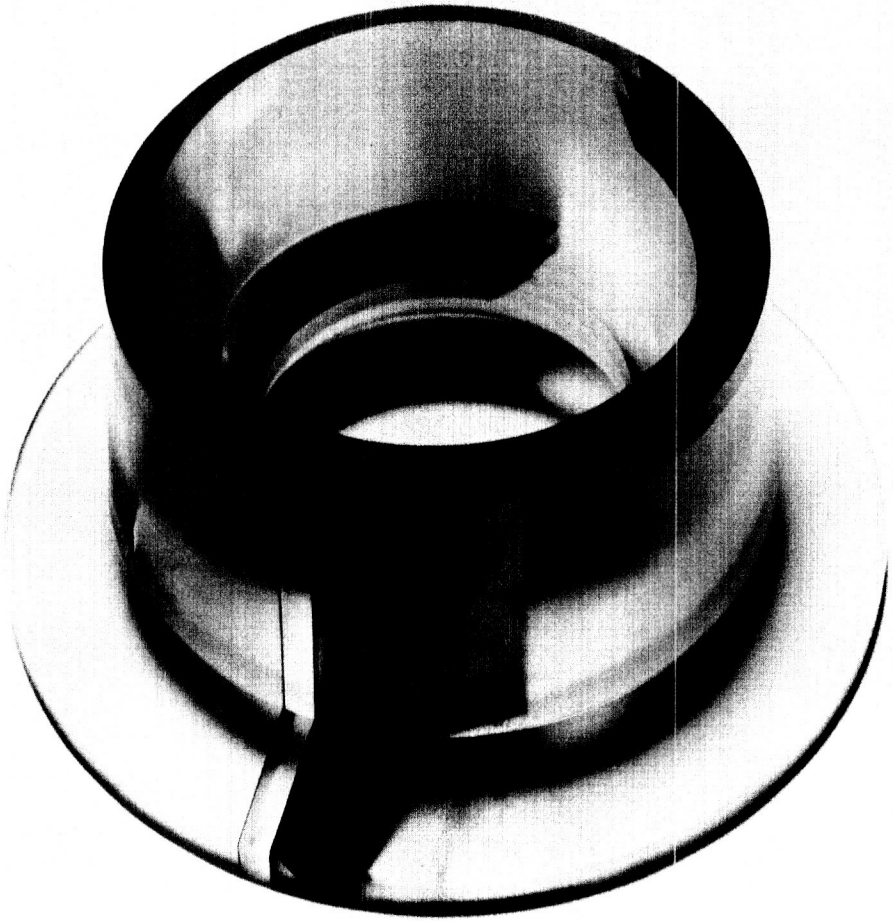

FIG. 40

FINISHED THROAT SECTION

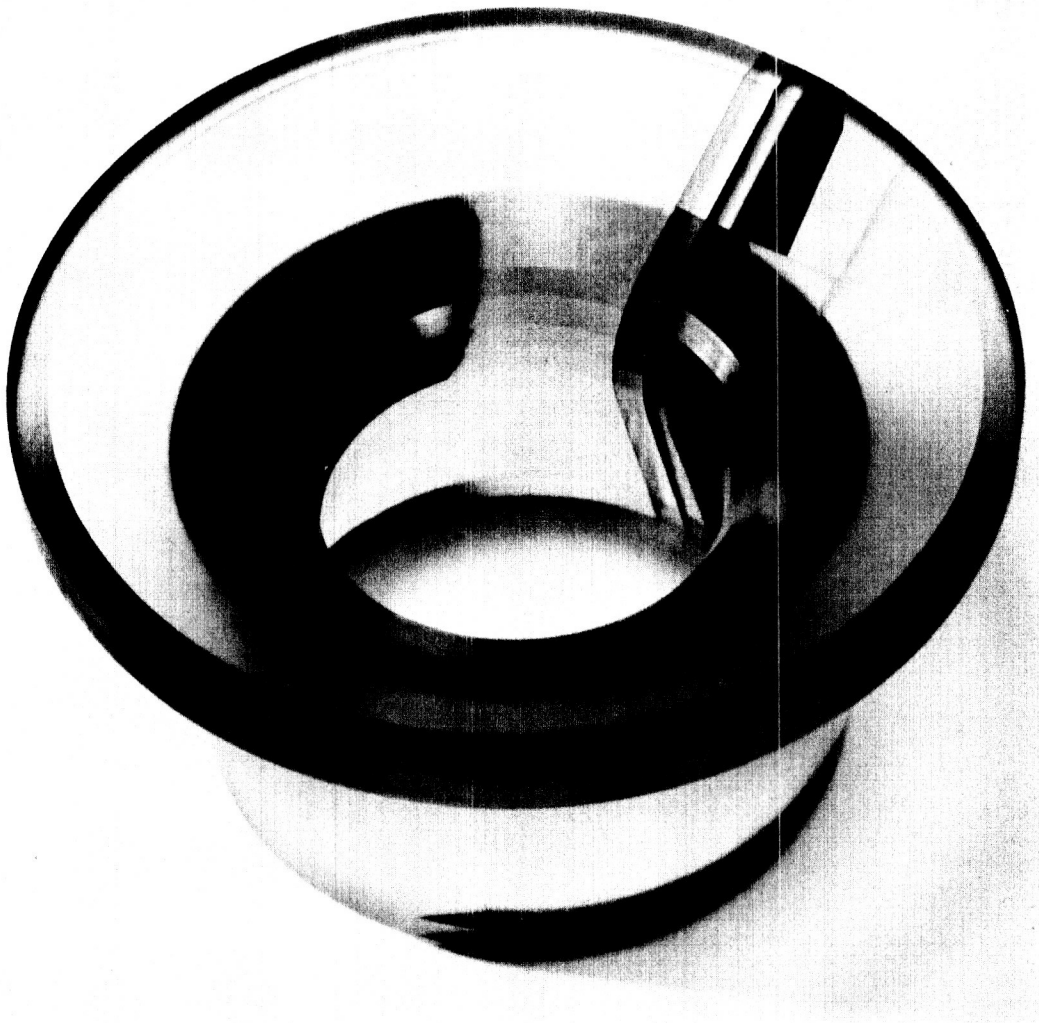

FIG. 41

FINISHED THROAT SECTION

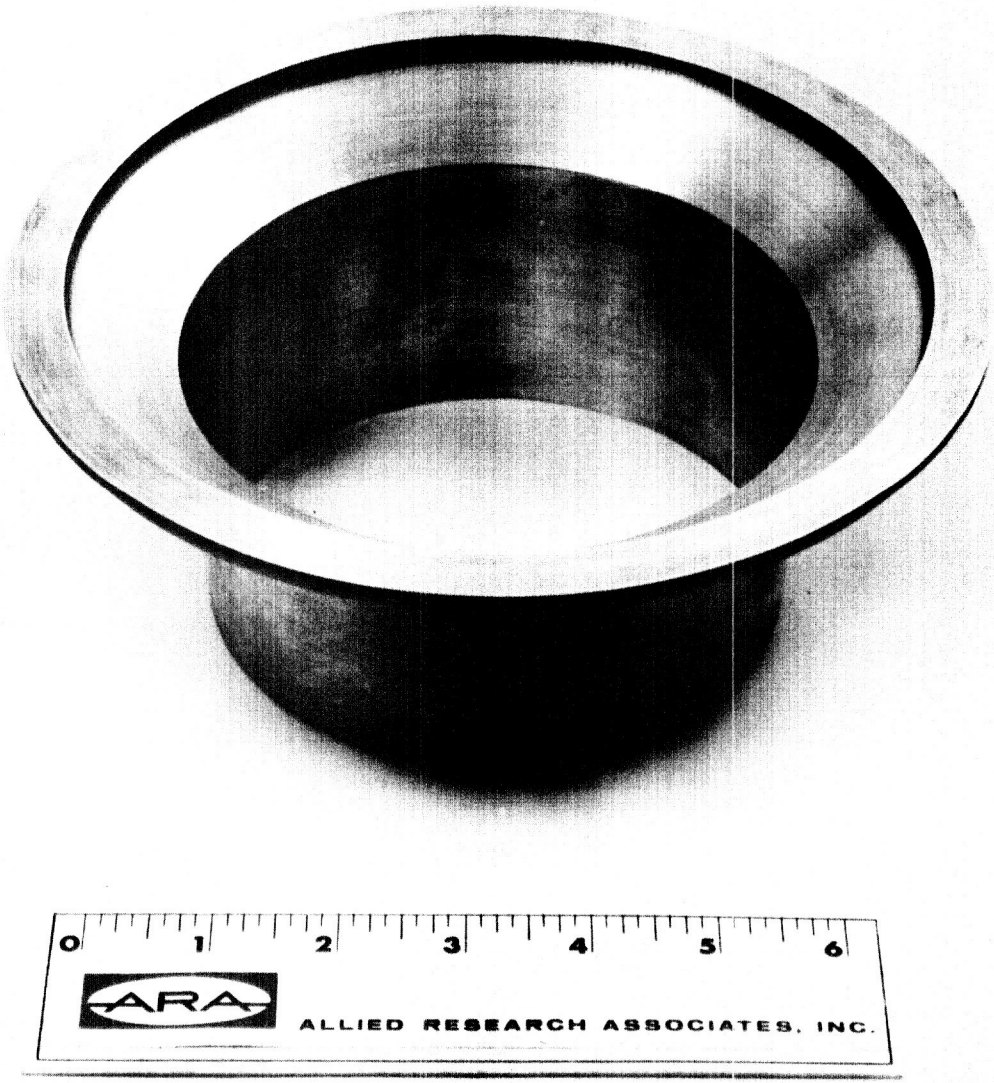


FIG. 42

MAGNESIUM REINFORCEMENT BLANK

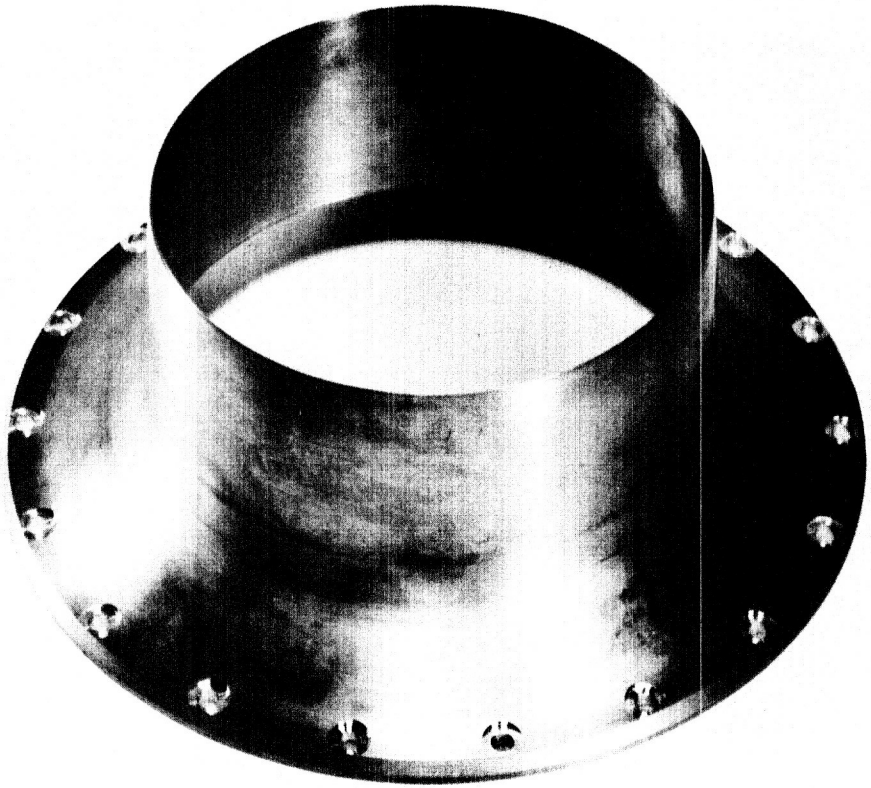

FIG. 43

FINISHED MAGNESIUM REINFORCEMENT


FIG. 44

# BLANK FOR EXPANSION SECTION OF NOZZLE

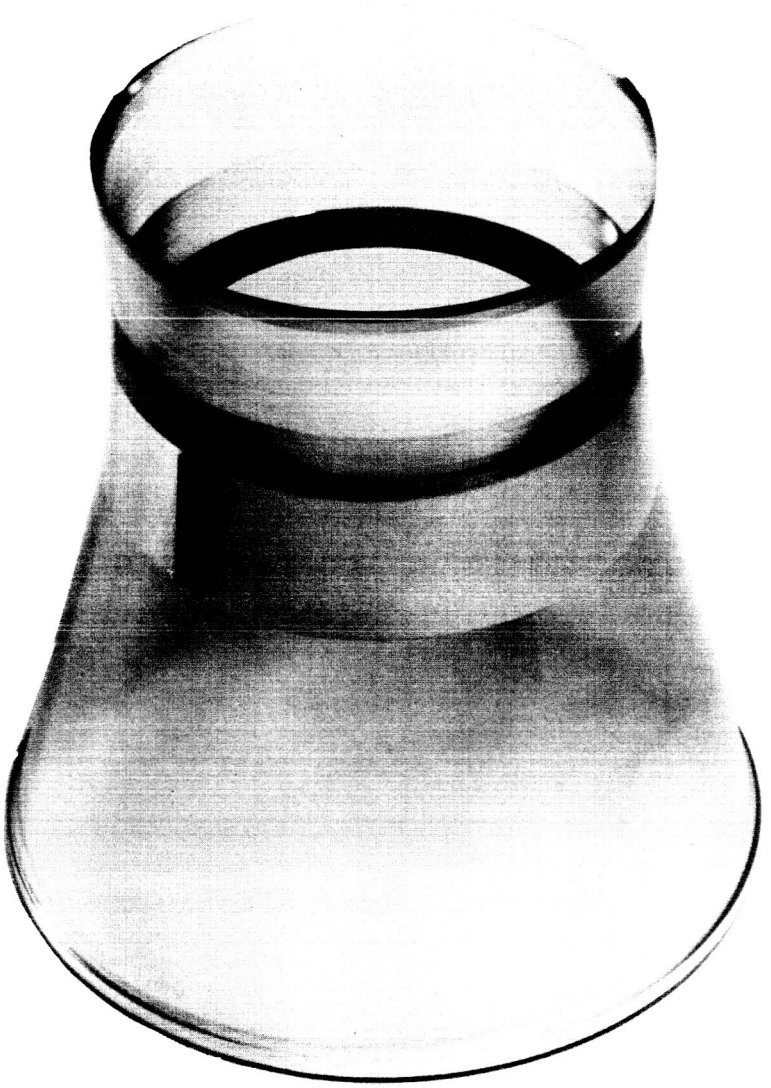

FIG. 45

FINISHED EXPANSION SECTION WITH LONGITUDINAL POLARISCOPE

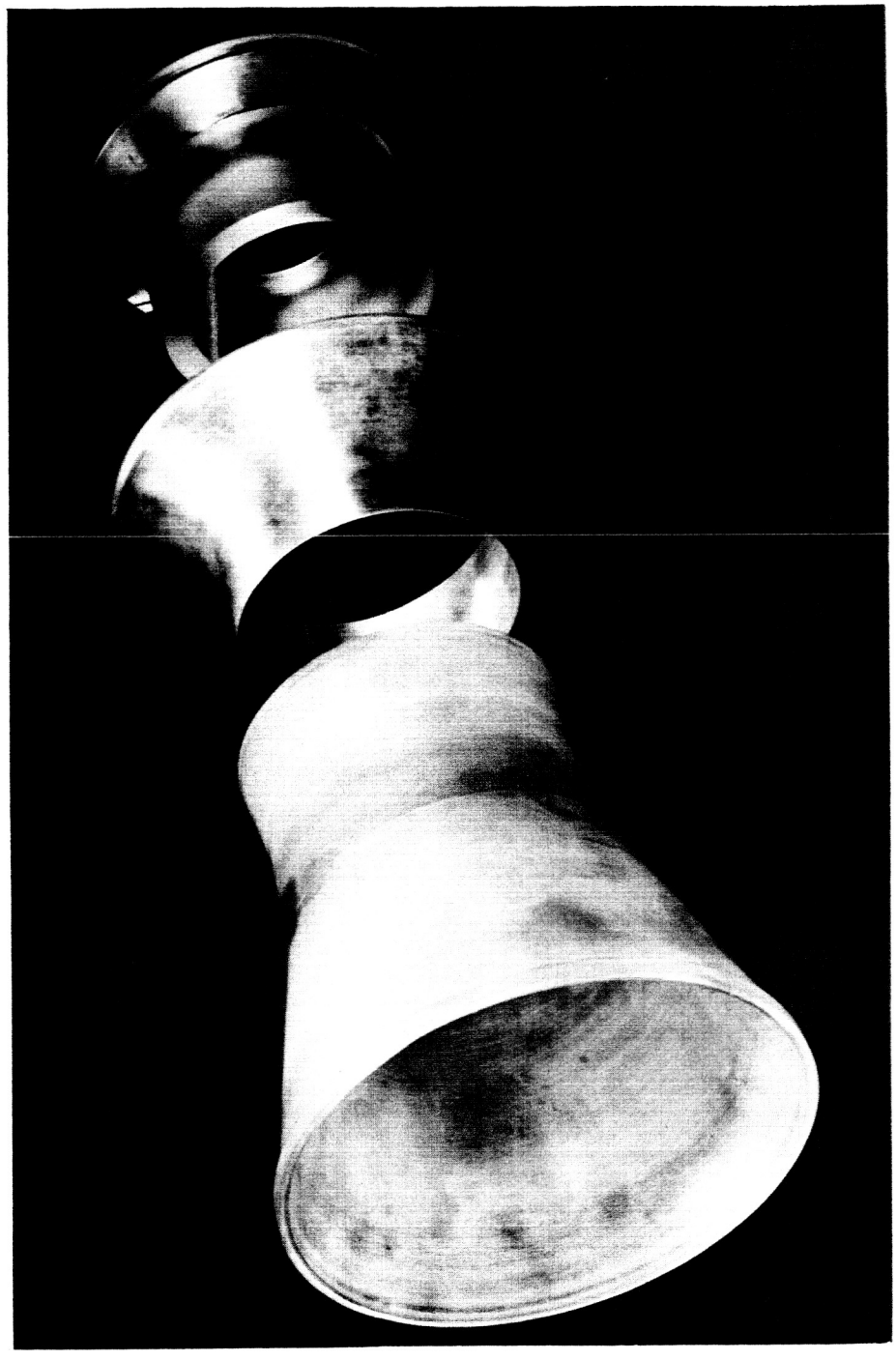

FIG. 46

ALGOL II B NOZZLE COMPONENTS

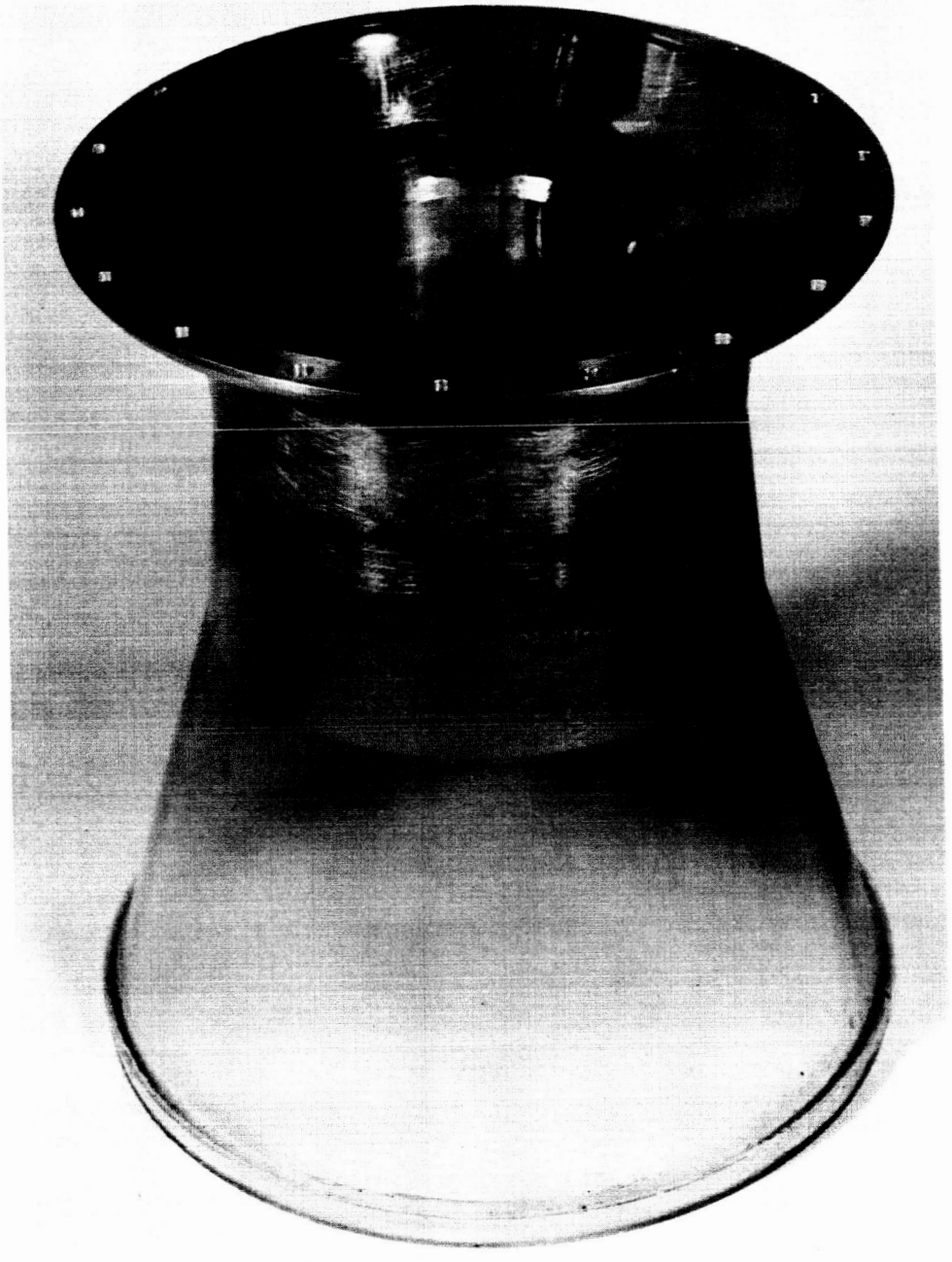

FIG. 47

COMPLETED ALGOL II B NOZZLE

FIG. 48

# PRESSURE CLOSURE IN THROAT

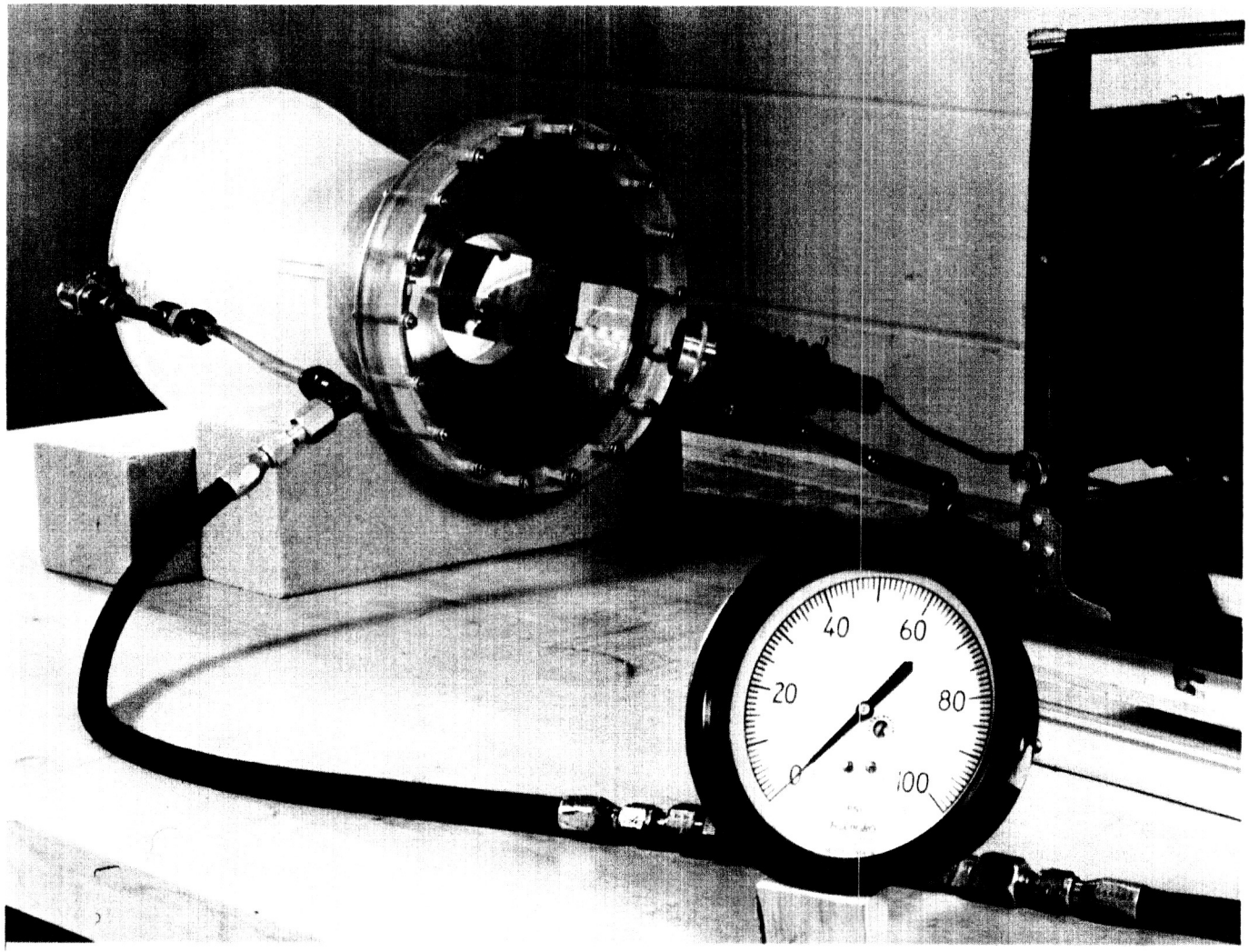


FIG. 49

TEST ARRANGEMENT FOR VIEWING CIRCUMFERENTIAL AND THROAT AREA POLARISCOPES

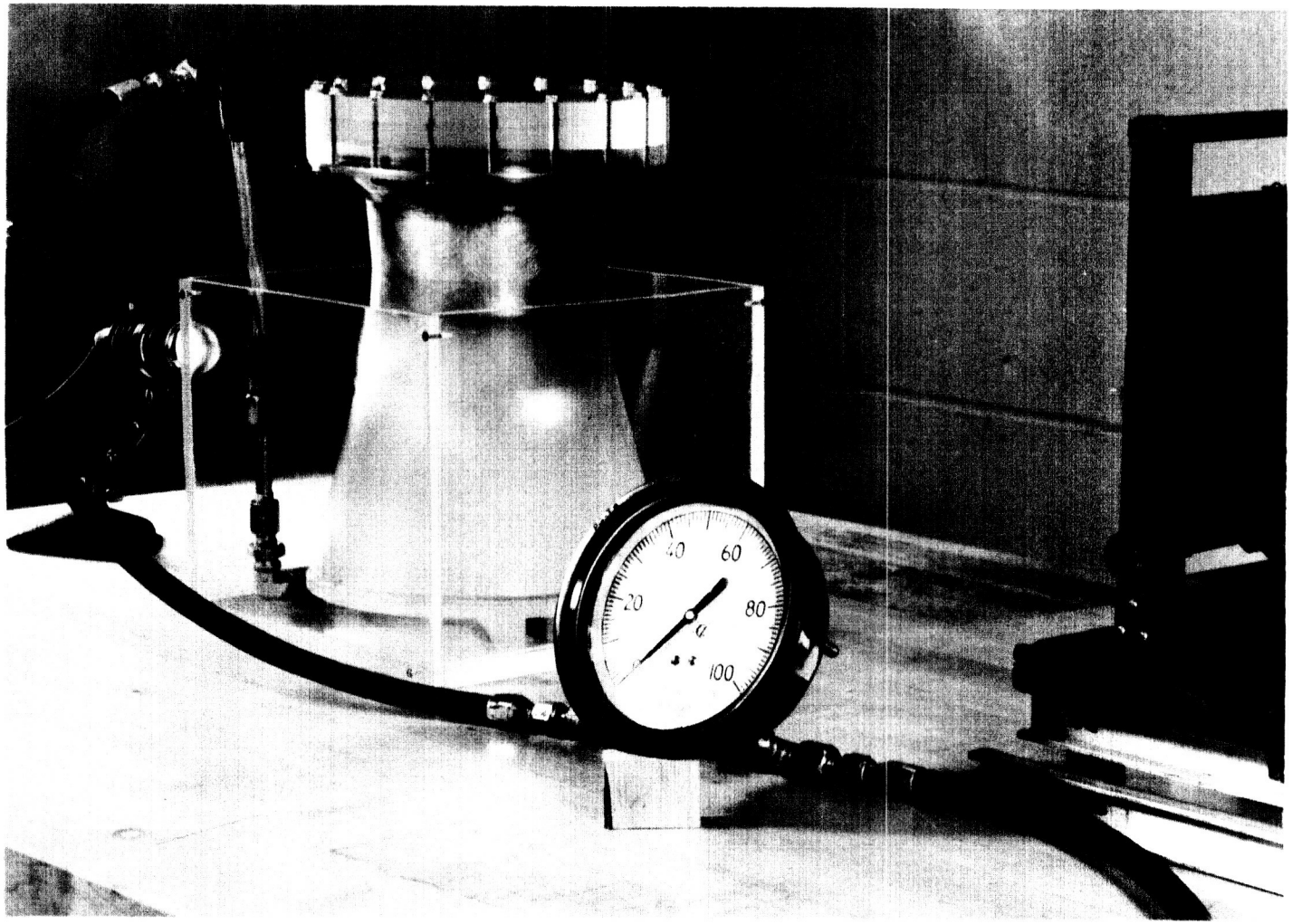


FIG. 50

TEST ARRANGEMENT FOR VIEWING
LONGITUDINAL POLARISCOPE
IN EXPANSION SECTION

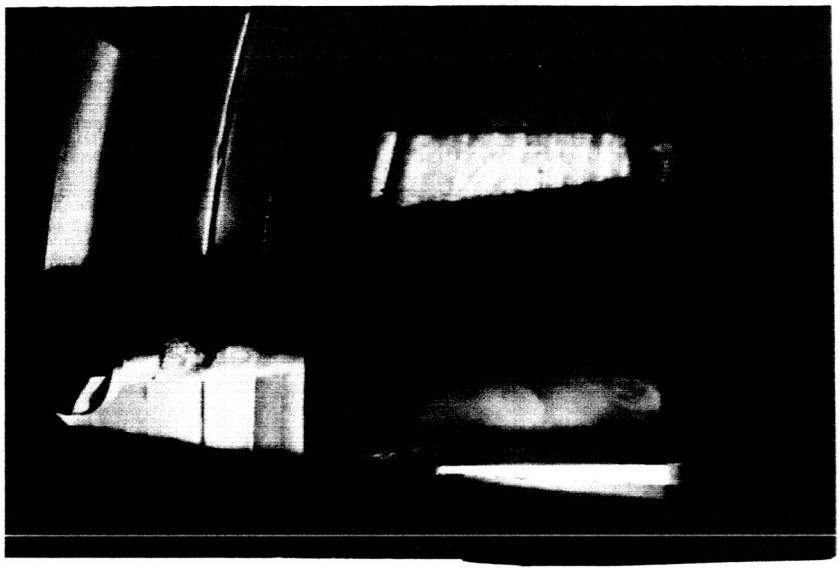

0 psi

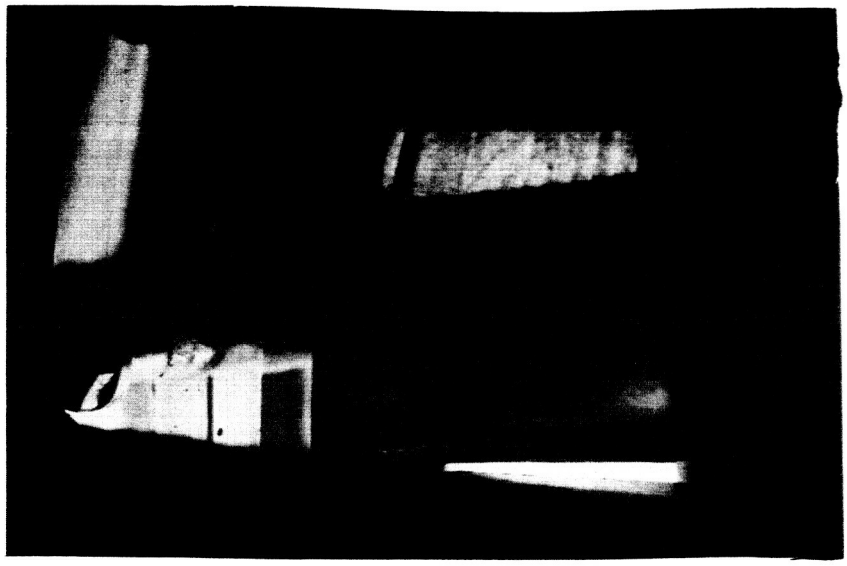

30 psi

FIG. 51

# STRESSES IN ENTRANCE SECTION

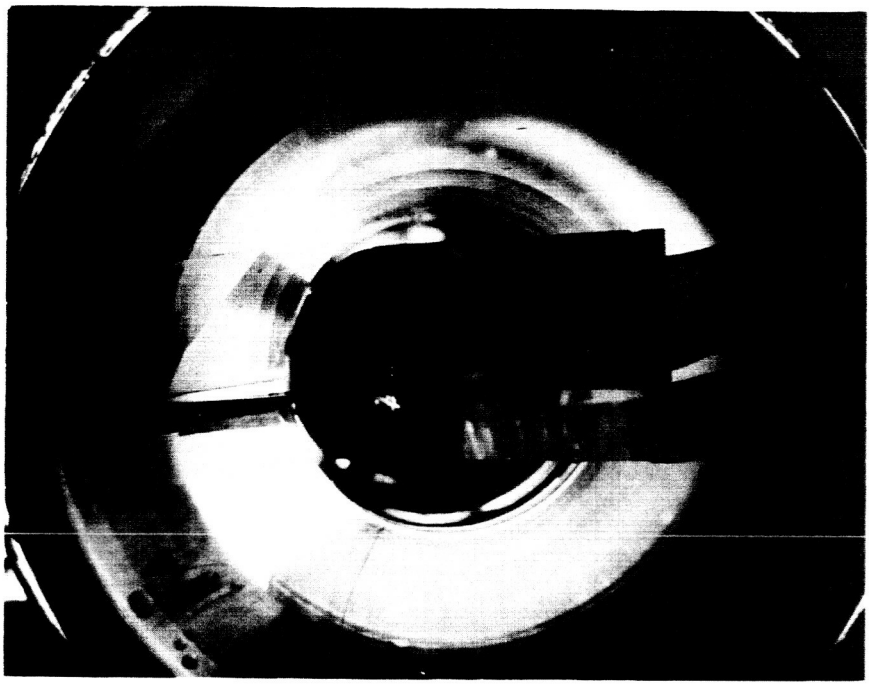

0 psi

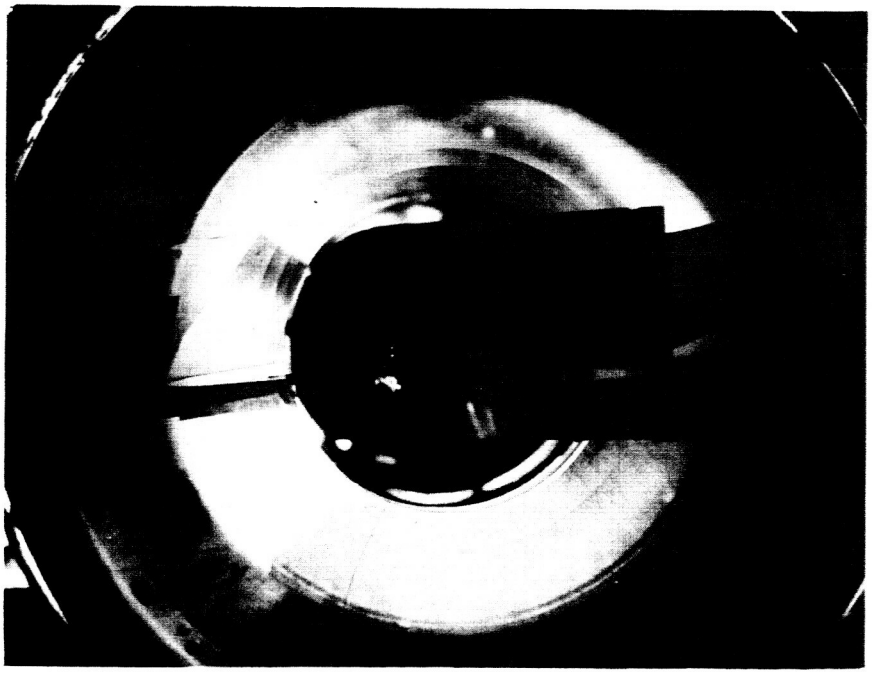

30 psi

FIG. 52

STRESSES AT CIRCUMFERENTIAL POLARISCOPES

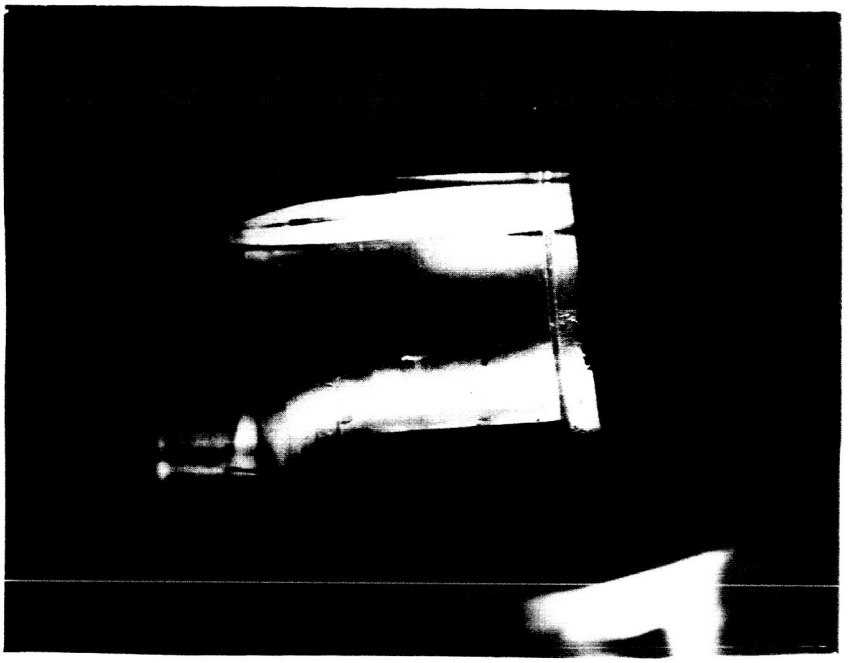

0 psi

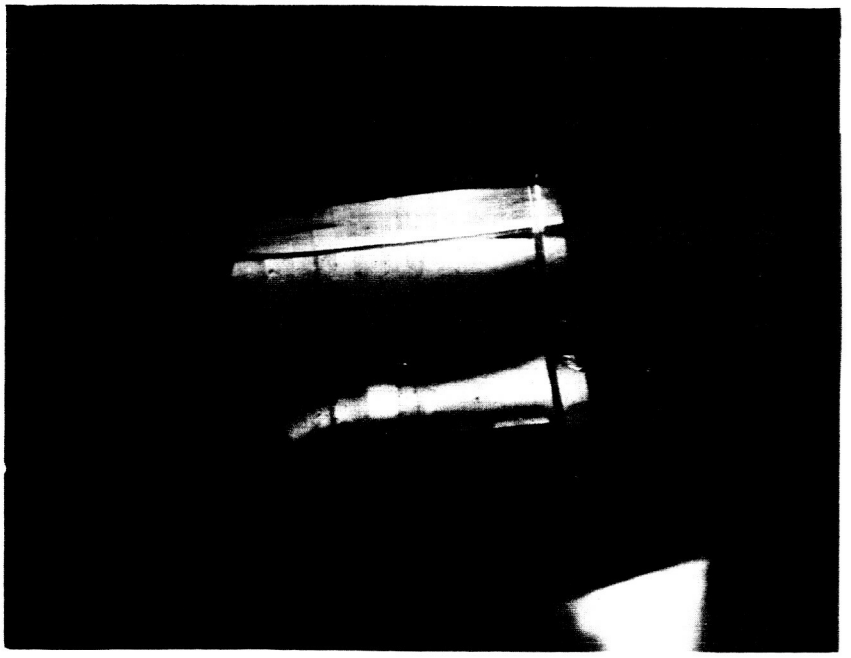

40 psi

FIG. 53

STRESS AT THROAT SECTION

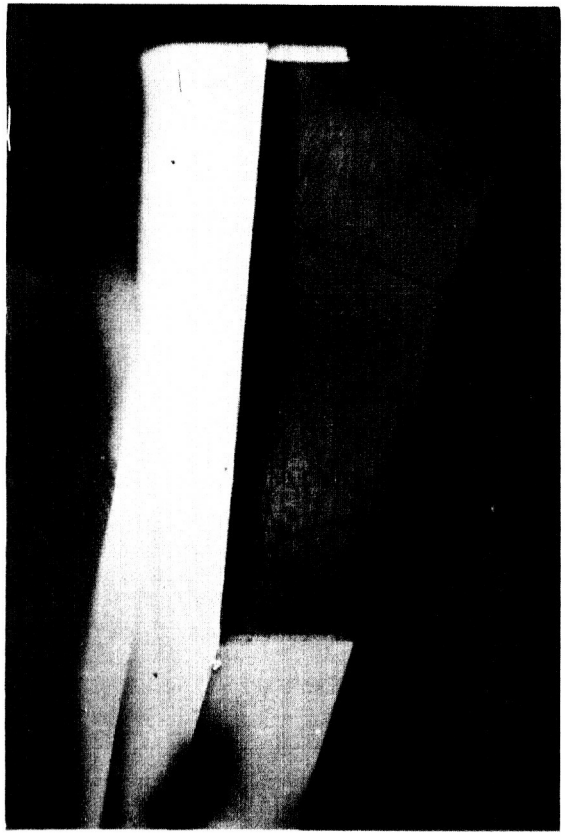

40 psi

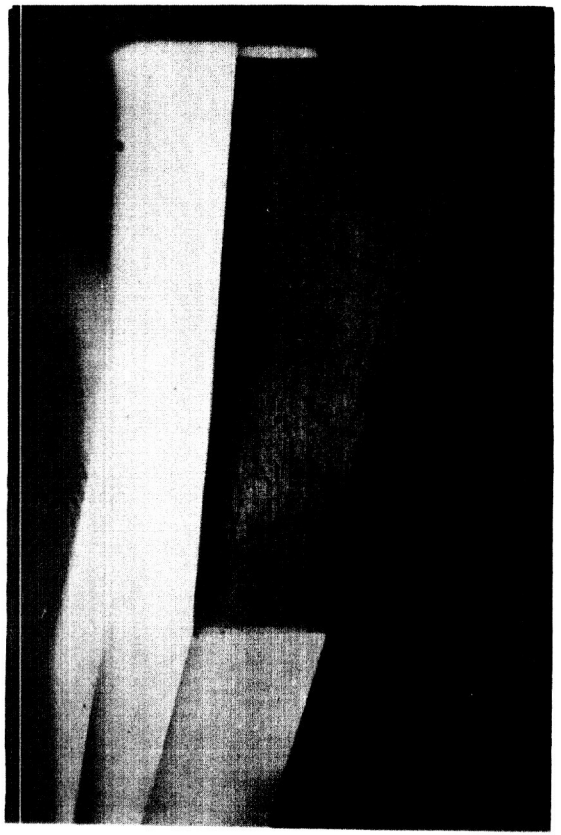

0 psi

FIG. 54

STRESSES AT EXPANSION SECTION

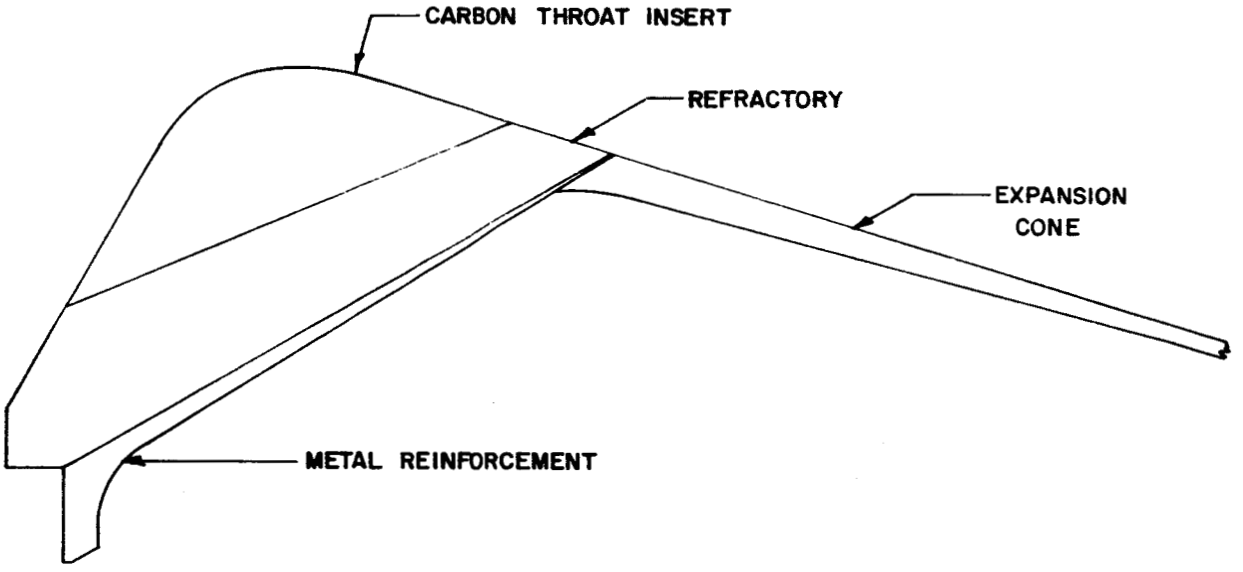


FIG. 55

# POSSIBLE NOZZLE REDESIGN CONCEPT